UNIVERSITÀ DEGLI STUDI DI FIRENZE
Facoltà di Scienze Matematiche, Fisiche e Naturali

Dottorato in Scienze Chimiche, Ciclo XXII

Ab initio molecular dynamics in condensed phase systems

Tesi di dottorato di:
Cristian Faralli

Tutore:
Vincenzo Schettino

Coordinatore:
Gianni Cardini

Settore disciplinare: CHIM/02 - Chimica Fisica

Contents

1 Introduction **1**

1.1 Molecular dynamics theory 3

1.2 Problems of condensed phase 5

2 Dynamics of ions in methanol solution **7**

2.1 Br^- 10

2.1.1 Results 11

2.1.2 Conclusions 14

2.2 Na^+ and K^+ 15

2.2.1 Results 16

2.2.2 Conclusions 21

2.3 Mg^{2+} and Ca^{2+} 21

2.3.1 Results 22

2.3.2 Conclusions 29

3 Parallelization of a code for Bader analysis **31**

3.1 Results 33

3.2 Conclusions 35

4 Fluorinated alcohols as stabilizing cosolvents **37**

4.1 Simulation details 38

4.2 Hexafluoroisopropanol results 39

4.3 Hexafluoroacetone results 50

4.4 A case study: melittin in hexafluoroisopropanol/water solution . . . 61

4.5 Conclusions 62

5 Open-addiction versus cyclo-condensation of organic compounds **65**

6 Conclusions **75**

1

Introduction

Pioneering works concerning Density Functional Theory (DFT) were presented in the middle of 70s by Hohenberg and Kohn[1] and by Kohn and Sham.[2] This happened 40 years after the celebrated success of the paper by Schröedinger,[3,4] giving the starting point to the wave mechanics. Actually, the first appoach to what will be subsequently called DFT was anticipated by Thomas and Fermi[5,6] with their studies on the atom properties but they received little consideration about it.[7] During the last 60 years, enormous advancements have been made to find approximated solutions to the Schröedinger equations for many-electrons systems, supported by the progressive improvement of the computer technologies.

Nowadays technology has deeply changed the way to lead the modern scientific research, thanks to the increasing adoption of computers as powerful investigation tools. Computer simulations explore the time evolution of an atomic system describing the behaviour on a very short time scale. In this way it is possible to have a detailed picture at the atomic level to explain the macroscopic properties of a system.[8]

Through the years researchers have found a number of applications of the Molecular Dynamics (MD), from astrophysics to material science, from polymers to biology,

with almost unlimited capabilities. The most important contribution to the application to chemical systems has been given by the use of DFT to model the interaction potential. This allows bond break and formation and it considers polarization effects and charge transfer. representing an alternate approach to the theory of the electronic structure. Instead of reasoning in terms of single-particle WaveFunction (WF) in the Hilbert multidimensional space, the DFT provides a different perspective targeting a real quantity in the three dimensional cartesian space, namely the electronic density, which assumes a more physical significance. In DFT methods the increase of the computational time as a function of the system dimensions is very moderate.

One of the most efficient method to obtain a realistic description of complex systems is based on the synergy of *ab initio* MD with the DFT in the Generalized Gradient Approximation (GGA). This approach needs a high computational effort, but the problem has been partly resolved by adopting Plane Waves (PWs) together with PseudoPotentials (PPs) to reduce the degrees of freedom. For every configuration, the necessary forces to evaluate the dynamics of the system are obtained by electronic structure calculations. The obtainment of the forces from first principles allows to overtake one of the most limiting factors of the classical MD that is the impossibility to have an accurate analitical potential to satisfactory describe highly polarized systems or chemical reactions with formation/break of bonds. A heavier computational load together with a more narrow temporal window of the phase space may represent slight shortcomings for the *ab initio* MD simulations with respect to classical approaches.

The combination of MD and DFT within the Car-Parrinello formalism[9–14] gives a powerful tool to successfully study complex chemical processes in condensed phase as it finds large applications for a great variety of systems.[15] *Ab initio* MD methodologies allow to investigate properties explicitly depending on electronic states such as IR spectra, Raman scattering or NMR chemical shifts.[12,16–18] Moreover, hybrid methods such as Quantum Mechanics/Molecular Mechanics simulations[12,19–27] permit to treat extended systems with a classical MD, limiting the *ab initio* calculation

to a more sensitive restricted region of the electronic density distribution. These kind of calculations[12] may be applied to classical MD of liquids, in which localized solvation centers are refined by *ab initio* level of theory. Metadynamics approaches allow to explore phase space separated by a high energy barriers in order to describe rare events[28,29] by *ab initio* MD, such as phase transitions under high pressure conditions.[30] Experimental difficulties are encountered in studying system under heavy pressure where molecular interactions are often hard to be comprehensible. Also polymerization or condensation in these extreme conditions[31] are often hard to be performed even though they are scientifically important for the research of new materials. By this way *ab initio* MD represents a very robust and useful method in order to foresee the behaviour of such systems which sometimes need expensive instruments and devices.

1.1 Molecular dynamics theory

The theoretical construct about classical molecular dynamics is plain.[32] A chemical system may be entirely described once the interaction potential $\phi(\mathbf{r_i})$ between particles is known. After that, the evolution of the ensemble may be argued by the Newton's equation of motion:

$$m_i \ddot{r}_i = -\frac{\partial \phi(\mathbf{r_i})}{\partial \mathbf{r_i}}$$

Several algorithms exists in order to find the numerical solution of this equation (for example Verlet). The potential is the only variable to evaluate and the choice of the interatomic forces is fundamental and it is carried out by setting parameters coming from previous experimental or theoretical data.

This method is not a robust predictive tool for strongly polarized systems or for the description of chemical reactivity between species where break and formation of bonds occurs. This problem is overtaken by Born-Oppenheimer (BO) MD where the forces acting on the nuclei are computed by first principles optimizing the electronic structure at every step of the MD simulation.

Only in the last 15 years computational developments have allowed, with the advent of *ab initio* MD, a determination of accurate potentials which are not empirically *a priori* determinined. In *ab initio* calculations the potentials are computed step by step during the evolution of the simulation according to the BO principle.

The exact calculation of the electronic ground state energy can not be achieved for many-electrons systems and approximations need to be considered.[33] This kind of computations are performed for every evolution step of the system in the *ab initio* methods. The DFT represents the balanced choice between time efficency and accuracy of the results. It is based on two principles: the first states that the energy of the ground state of a many-electrons system is described by an unique electronic density functional $E[\rho(\mathbf{r})]$.[1] The second theorem gives a practical way to calculate the ground state energy with the electronic density as a sum of singularly occupied orbitals:[2]

$$\rho(\mathbf{r}) = \sum_{occ} \Psi_i^*(\mathbf{r})\Psi_i(\mathbf{r})$$

The energy functional $E[\rho(\mathbf{r})]$ that describes the system is:

$$E[\rho(\mathbf{r})] = -\frac{1}{2}\sum_{occ}\int \Psi_i^*(\mathbf{r})\nabla^2\Psi_i(\mathbf{r})d\mathbf{r} + \int \rho(\mathbf{r})V_{ext}(\mathbf{r})d\mathbf{r} + \int \rho(\mathbf{r})V_H(\mathbf{r})d\mathbf{r} + E_{xc}[\rho(\mathbf{r})]$$

Apart from the nuclear interactions $U(\mathbf{R})$, it is made up by the kinetic energy contribution $-\frac{1}{2}\nabla^2$, the interaction between electrons and external potential generated from the nuclei $V_{ext}(\mathbf{r})$, the Coulombian interaction $V_H(\mathbf{r}) = \int \frac{\rho(\mathbf{r}')}{|\mathbf{r}-\mathbf{r}'|}d\mathbf{r}'$ and the exchange-correlation functional $E_{xc}[\rho(\mathbf{r})]$ which has an unknown formulation but there are very accurate approximations for it. So we have:

$$[-\frac{1}{2}\nabla^2 + V_{ext}(\mathbf{r}) + V_H(\mathbf{r}) + V_{xc}(\mathbf{r})]\Psi_i(\mathbf{r}) = \varepsilon_i\Psi_i(\mathbf{r}) \tag{1.1}$$

where $V_{xc} = \frac{\delta E_{xc}[\rho(\mathbf{r})]}{\delta\rho(\mathbf{r})}$

The most diffused way to describe the $E_{xc}[\rho(\mathbf{r})]$ functional is the Local Density Approximation (LDA) which contains the exchange-correlation potential of an uniform electron gas and it allows to obtain accurate geometric properties. The LDA is valid when little and slow electronic density variations occur as it happens for most of the systems. The GGA has been lately adopted as an alternate model

for exchange-correlation contribution. It contains also a dependence on the density gradient and it allows a more detailed description of bond energies and hydrogen bonds than LDA.

In order to improve the computational efficency, an extended Lagrangian method has been proposed by Car and Parrinello,[11] instead of resolving the Kohn-Sham equations. It is possible to successfully ignore the WFs which describe the core electrons because they do not intensively partecipate to chemical processes such as bond formation. The description of these inner electrons has been substituted by PPs with a decrease in the number of particles to be treated and a consequent improvement of the computational yield. Moreover PPs allow for an accurate description because of the difficulty to follow the rapid oscillations of the electrons near the atoms and most of the chemical processes involve valence electrons which are instead correctly represented. The resolution of the Eq. 1.1 is performed by adopting either PWs and PPs. The convergence of the self-consistent computations is easly controlled by varying the expansion of the PWs. The Pulay forces are also neglected because PW expansion does not depend on atom positions.

Car and Parrinello have developed an efficient method[11] to follow the dynamics of an ensemble of ions and electrons with two different energy scales according to the BO approximation. The ions move at a certain temperature and the electrons have to adiabatically follow them remaining in an instantaneous ground state. In this context ions and electrons have a classical treatment and they are described by a Lagrangian which will contain the fictitious mass of the electrons in order to solve their time evolution on the BO surface.

1.2 Problems of condensed phase

In this work successful applications of *ab initio* MD simulations within the Car-Parrinello formalism together with classical MD simulations have been performed to rationalize chemical-physics problems of condensed phase. The arguments will be separately described as in the following.

In the Chap. 2 the solvation dynamics of ions in methanol solutions has been studied with a particular attention to the solvation shells. Different kind of interactions have been taken into account with the study of the Br^- anion, the monovalent Na^+ and K^+ cations, and the bivalent Mg^{2+} and Ca^{2+} cations. Polarization and charge transfer effects have been investigated and the first shell contribution has been put in evidence.

In the Chap. 3 the parallelization of an algorithm for the Bader charge calculation has been performed with a *Master-Slave* strategy to obtain more accurate results for the charge transfer in shorter computational times. Charge transfer is a very important property for highly charged systems such as ionic solutions and a parallelization is necessary since a large number of configurations has to be analyzed.

In the Chap. 4 both *ab initio* and classical MD simulations have been performed to study the effects of fluoroalcohols in water solution in stabilizing the secondary structure of short polypeptides. Starting from the structural and the electronic properties of *ab initio* simulations, a new and reliable force field has been constructed and classical MD simulations have been performed. Solvation properties and clustering reorganization of the solvents have been investigated in order to understand the effects of fluoroalcohols on the secondary structure of proteins.

In the Chap. 5 "all electrons" optimization of structures has been performed by *ab initio* calculation on organic compounds to explain the reaction mechanism of nitro compounds with electron-deficient olefins and to understand the role of Cu^{2+} in addressing selectively the reaction path.

2

Dynamics of ions in methanol solution

The Molecular Dynamics (MD) simulation study of liquid methanol[34] gives a quite exaustive view of a strongly self-associating liquid. Methanol has a wide biochemical interest and in the last few years the attention on this solvent has also grown in technological matter as a possible fuel cell component.[35–39] Since it is the representative molecule of the alcohol series, methanol is the simplest organic solvent which contains both a hydrophilic (OH) and a hydrophobic (CH_3) group. The pure liquid forms an extended H-bond network which mainly gives rise to chain structures and bifurcated interactions.[34] The presence of weaker directional H-bond of the C-H$\cdots$O type increases the complexity of the aggregation of the liquid. Despite its semplicity and importance, the number of computational studies on the structural and dynamical properties of the liquid[23,34,40–47] is limited.

The interaction of ions with methanol strongly affects colligative properties of the solution, together with reactivity and many phenomena of technological[35–39] and biochemical interest. For some ions, the stability of the solvation shell may affect properties of the solution, eliminating the molecules of the first solvation shell. The diffusion properties of the ions will be affected since the molecules of the first solvation shell will diffuse with the ion increasing their effective radius. This stability

will also have consequences on the reactivity of these species in solution since the presence of ions can strongly perturb the structure of the liquid. A particular role is played by the stability of the first solvation shell although in some cases the perturbation extends farther away from the ion.

The interaction between the halide ions and the methanol molecules occurs via the formation of H-bonds,[48,49] while the interaction with cations is predominantly electrostatic.[50,51] Nevertheless methanol is very attractive for both theoretical investigations and experimental standpoints because of the number of solvent molecules involved in this interactions that is still a matter of debate.[52–57]

In order to obtain useful insight on the structural and dynamical properties of ions in solution a series of experimental methods[58] has been applied, such as X-ray and neutron scattering or infrared and Raman spectroscopy and, more recently, femtosecond techniques.[59–65] On the other side, it has been proved that theoretical methods[66–69] such as high level *ab initio* computations,[70–80] Monte Carlo ensembling[81–86] and MD simulations[87–105] are powerful tools to give insights also on properties difficult to be addressed experimentally.

Many investigations have been performed to analyze water as solvent[46,97–99,106–125] with a minor interest to other molecules. Only a limited attention has been devoted to ions solvation in other solvents like methanol,[48,49,81,126–129] acetonitrile,[130] tetrahydrofuran,[81] acetone[131,132] or ammonia[116,133,134] where a large interest due to physical and chemical implications in a wide range of research and technological fields keeps growing and where the knowledge of important properties of the first solvation shell is still incomplete.

The interactions of ions with polar solvents are not simple to be modeled using semiempirical potentials because of the strong polarization of the first solvation shell and the charge transfer which may occurs between solvent molecules.[48,49,83,89,94,100,108,112,135,136] It has been recently observed[83,89,94,100,102,135,136] that the semiempirical potentials usually adopted in classical molecular dynamics or Monte Carlo simulations do not reproduce the coordination number accurately, since polarization and charge transfer effects are not taken properly into account.

These problems have been overcome to a good extent by first principles molecular dynamics simulations that explicitly consider the fluctuations of the electron density. These ionic systems have been successfully approached using *ab initio* MD employing Density Functional Theory (DFT) in the generalized gradient approximation. The reliability in modelling the ion-methanol interaction has been confirmed comparing the results to calculations on clusters at the MP2 level of theory with a localized Gaussian basis set.[48–51] *Ab initio* MD requires considerable computational resources that limits the system size and the length of the phase space exploration but at the same time it comes out to be a powerful tool to achieve an accurate description of chemical systems. A powerful approach to tackle these troubles is offered by Quantum Mechanics/Molecular Mechanics methods that allows to consider a small part of the system to a high level of theory, treating the rest with semi-empirical potential in order to reduce the overall computational load.

A systematic series of study has been carried out in order to understand the role of simple ions in describing the behaviour of methanol as a solvent. Particular attention has been paid for the Br^-ion[49] in comparison with another important anion such as Cl^-.[48] Alkaline ions[50] such as $Na^+$and K^+ and alkaline-earth ions[51] such as $Mg^{2+}$and Ca^{2+} have been taken into account subsequently, putting in evidence the differences between species of the same group in the periodic table. The main results obtained from these studies deal with the structure of the solvent in the first solvation shell and its stability,[123] the charge transfer and the H-bond formation between ions and solvent molecules. The structure of the solutions has been mainly analyzed with pair distribution functions. The electronic properties have been obtained on the basis of the Maximally-Localized Wannier Functions (MLWF)[137–140] in order to obtain an accurate description of the dipole moments with the Wannier Function Centers (WFCs). The position of the WFCs is directly related to the position of the electrons in the system and, as a consequence, it is possible to compute the molecular dipole moment assuming that these electrons belong to the nearest neighbor atom, giving an average description of the polarization that characterizes the system. The Atoms In Molecules (AIM) electronic population analysis with the

widely applied method[141–148] proposed by Bader[149–151] has been adopted to evaluate the charge transfer due to the presence of the ionic center, and the electronic redistribution upon the solvent molecules as a function of their distance from the ion.

In the following sections of the chapter it is shown that a satisfactory discussion of the general properties of methanol solutions can be appropriately based on the results for for the simple ions taken into account. All results and discussions reported below have been already dealt with in previous works and have been published in international chemical-physics journals. Data on Br^- are found in "Structure and dynamics of Br^- ion in liquid methanol"[49] (The Journal of Physical Chemistry B 2006, **110(30)**, pages: 14923-14928); results on monovalent ions are discussed in "The solvation dynamics of Na^+ and K^+ ions in liquid methanol"[50] (Theoretical Chemistry Accounts 2007, **118**, pages: 417-423) whereas divalent ions are examined in "Ab Initio Molecular Dynamics Study of Mg^{2+} and Ca^{2+} Ions in Liquid Methanol"[51] (Journal of Chemical Theory and Computation 2008, **4(1)**, pages: 156-163).

2.1 Br^-

The structural and dynamical properties on a solution of bromide ion in liquid methanol[49] have been analyzed with Car-Parrinello Molecular Dynamics (CPMD) and compared with those of Cl^-obtained by previous simulations[48] and for the bromide in water,[152,153] allowing for an accurate comparison of the solvent effects.

In a recent work[48] it has been shown that CPMD simulations reproduce the coordination number for the chloride ion in methanol correctly (3.56), since polarization effects, charge transfer and hydrogen bond are accurately described. In this work the method has been extended to the bromide ion in methanol. This is of particular interest since the experimental data[53,54,154] are not exhaustive as in the case of the chloride.

The first solvation shell has been characterized in terms of H-bonds showing

that the high polarization of the bromide gives rise to a stable solvent cage. The different coordinative trend with respect to the chloride can be attributed to the ionic radius and to the stronger perturbations brought by the solvent to the bromide. A particular attention has been devoted to polarization and charge transfer in the formation of the H-bond between bromide and the methanol solvent, since it has been found that stability and morphology of the first solvation shell are very sensitive with regard to this electronic effects.[48,49]

2.1.1 Results

It is well known that the methanol molecules interact with the halide ions through H-bonds.[48,52,53,56,73,88,89,154] A snapshot taken during the present simulation of the first solvation shell is reported in Fig. 2.1b and shows the Br^- ion surrounded by four hydrogen bonded methanol molecules.

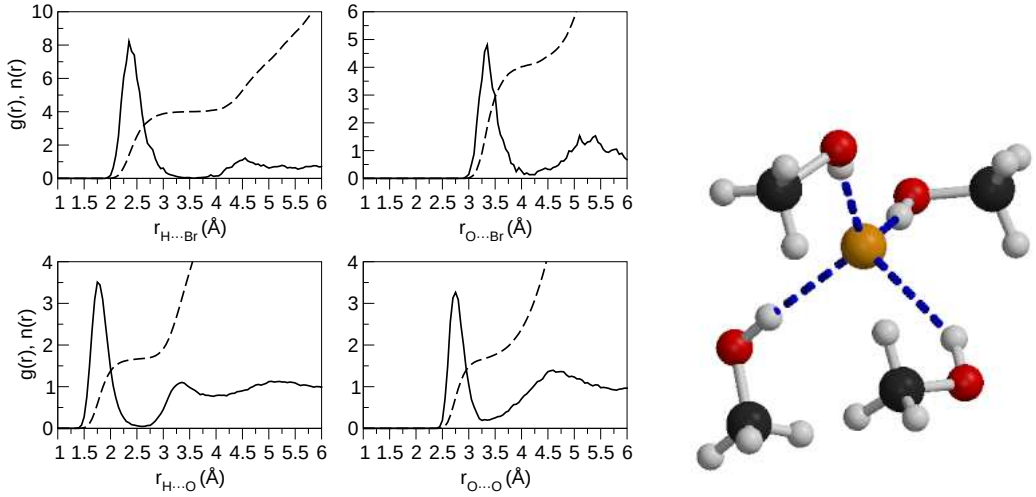

Figure 2.1: a) Upper panel: pair radial distribution functions (full) and running integration number (dotted) for the H$\cdots$Br (left) and O$\cdots$Br (right) contacts. Lower panel: pair radial distribution functions for the H$\cdots$O (left) and O$\cdots$O (right) contacts. b) Snapshot of the first solvation shell extracted from the CPMD simulation. The bromide-methanol interaction occurs through H-bonds.

The solvent reorganization can be more clearly observed from the pair radial distribution functions, g(r), related to the H$\cdots$Br and O$\cdots$Br contacts, reported in the upper panels of Fig. 2.1a. The coordination number for the bromide ion obtained from the $g_{H\cdots Br}(r)$ is of 4.01. This value compares very well with experiments[53,154] (3.7), whereas is much lower than values obtained by classical simulations considering hexa-coordination.[54] The absence of polarization effects leads to an incorrect picture of the first solvation shell and to larger coordination numbers[89] than expected. On the other side values of the coordination number in methanol lower than those in water[152,153] are expected due to the larger dimensions of the methanol molecule. In fact, in previous CPMD simulations in water, a coordination number of $\sim$5 for Cl^- ion[155–157] and $\sim$6 for Br^- ion[152,153] has been found. The O$\cdots$O and O$\cdots$H pair correlation functions are also reported in the lower panel of Fig. 2.1b to show the overlap of the solute-solvent and solvent-solvent contacts in the experimental data.[54]

A clear representation of the H-bond configurational space can be achieved through the pair radial and angular distribution functions, $g(r,\theta)$[34,158] reported in Fig 2.2.

The surfaces spanned by the H-bond of the bromide ion are very close to those of the chloride ion,[48] apart from the X$\cdots$H distance (with X=Cl or Br). Differences arise from the respective ionic radii (1.81 for Cl^- and 1.96 for Br^-). The behaviour of the methanol molecules in the first solvation shell is quite different. For the bromide ion a rather stable cage of four methanol molecules is present during the simulation, whereas the chloride ion interacts with a number of solvent molecules that ranges from two to five.[48]

Since the differences between the bromide and chloride ions are bound to the ionic radii and to the coordination number, a slightly different behaviour can be expected also for the related electronic structure properties like the charge transfer and the polarization effect. The charge transferred from the bromide ion as a function of the distance of the center of mass of the solvent molecules is reported in Fig. 2.3a. The charge transferred by Cl^- and Br^- ions is very close ($\Delta q(e^-)=0.24 \pm 0.02$ for

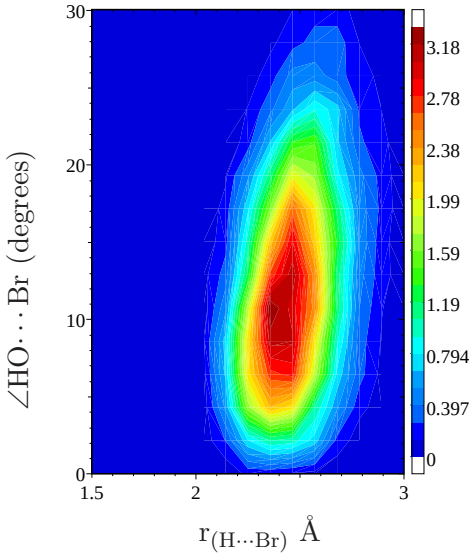

Figure 2.2: Weighted g(r,θ) function for the OH$\cdots$Br interactions for the H-bond characterization.[34,158]

Cl^- and 0.28 $\pm$ 0.02 the for Br^-) and it is essentially localized on the first shell molecules as evident from the distributions. This behaviour can be easily justified on the basis of the H-bond interactions between the ion and the first solvation shell molecules.

A description of the charge flow from the ion to first shell molecules can be obtained from the differences between the electron densities, $\Delta\rho$ as shown in Fig. 2.4.

In this qualitative description also H-bonds and polarization effects have to be considered and may concur to the perturbation of the charge density. However, it is clear that the ion-solvent interaction is mainly localized in the first solvation shell.

The polarization effects and in particular the dipole moment of the methanol molecules have been computed from the WFCs describing wavefunctions in terms of MLWF. However, as observed for the charge transfer, the dipole moment distributions of the first solvation shell molecules are very close (2.44 D for Cl^- and 2.41 D for Br^-)[49] with a lower average dipole moment by $\sim$0.2 D with respect to the

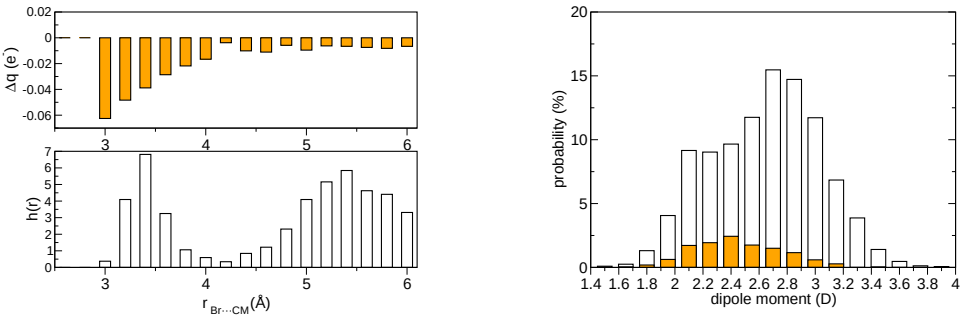

a) b)

Figure 2.3: a) Charge transfer $\Delta q(e^-)$ (upper panel) and non-normalized g(r) (lower panel) as a function of the $r_{Br\cdots CM}$ distance, where CM is the center of mass of methanol. b) Dipole moment distribution for the methanol molecules: the colored bars refer to the dipole moment distribution of the first solvation shell molecules, the white bars describe the second shell molecules.

average value found for the pure solvent (2.64 D). The dipole moment of the second shell molecules is quite similar to that of the pure solvent, confirming once again that the ion-solvent interaction is essentially localized in the first solvation shell, as reported in Fig. 2.3b.

2.1.2 Conclusions

The structural properties of the Br^- ion in methanol have been studied with CPMD simulations. The investigations have been mainly focused on electronic properties with an exhaustive characterization of the H-bond interactions between the first solvation shell and the ion. The bromide ion is surrounded by four methanol molecules that give rise to a stable cage. It has been observed, from the AIM population analysis and density of charge redistribution, that the ion-solvent interactions are essentially localized in the first shell region. The charge flows from the ion to the solvent molecules through the H-bonds so that the ion is strongly perturbed by the presence of the solvent as shown by the WFCs analysis, whereas a lower perturbation occurs for the solvent molecules of the first solvation shell.

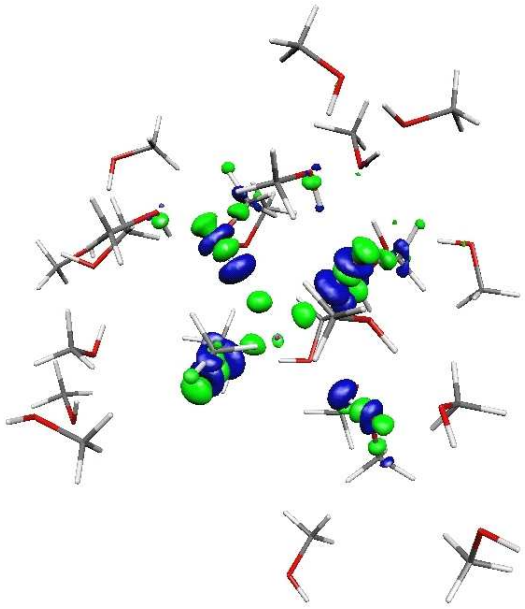

Figure 2.4: Density difference isosurfaces: $\Delta\rho$ at $\pm$ 0.003 (au) for the bromide solution ($\Delta\rho = \rho_{ion+solvent} - (\rho_{ion} + \rho_{solvent})$). Volumes with negative values are shown in green, volumes with positive values are in blue.

2.2 Na^+ and K^+

The structural and dynamical aspects of the solvation shell of Na^+ and K^+ in fully deuterated liquid methanol[50] has been studied by *ab initio* CPMD simulations. The results have been compared with those obtained from a previous work on Li^+ in the same solvent.[48] An increase of the coordination number going from Li^+ to K^+ together with a reduced stability of the cage around the ion have been ascribed to the increase in the ionic radius. A relatively more stable cage has been found for Na^+ than for K^+ and this property has been explained by means of electronic contributions, since it has been shown that charge transfer and polarization effects are significant in the solvation process of Li^+ in methanol.[48] By the way, an extension of the *ab initio* simulations to Na^+ and K^+ solvation will allow to build a fulfilled framework to draw a more complete picture of the solvation process of alkaline ions as a function of the ion dimension.

2.2.1 Results

Salient structural data (first peak position and coordination number in the ion-oxygen pair radial distribution functions) are reported in Table 2.1 and compared with classical MD results.[131,159]

	Na^+		K^+	
	first peak	n(r)	first peak	n(r)
	2.40	5.00	2.70	5.41
Marrone *et al.*[159]	2.55	5.5	2.95	6
Kim[131]	2.5	6.0	2.7	6.1

Table 2.1: First peak position (Å) and integration number from the pair distribution functions of Na^+ and K^+. The last two lines refer to classical MD simulations.

As in the case of the Li^+ in liquid methanol[48] the coordination number of the alkali metal ions obtained by CPMD is lower than found by classical MD, suggesting that the charge transfer and polarization effects play an important role in the overall description of the solute-solvent interactions.[48,89,94] Instead the first peak position in the ion-oxygen pair radial distribution functions appears to be quite independent of the model adopted, as observed in the CPMD studies of the same ions in water.[160,161] It is important to note that the coordination number obtained with CPMD simulations for both ions in methanol is lower than the corresponding value in water, essentially due to the greater steric effects of the CH_3 group of methanol. In fact the coordination number in water for Na^+ and K^+ are 5.2 and 6.75, respectively.[50]

The interaction of cations with methanol is mainly of electrostatic nature and the dipole moment of the methanol points toward the ion. In fact in the pair radial distribution functions (shown in Fig. 2.5a) the oxygen atom is the closest to the ions. This implies that the oxygen lone pairs are on the side of the ion and this will favor the charge transfer from the solvent to the ion.

It can be seen from Fig. 2.5a that the distance of the first peak in the g(r) increases with increasing ionic radius; this will lead to an increase of the coordination

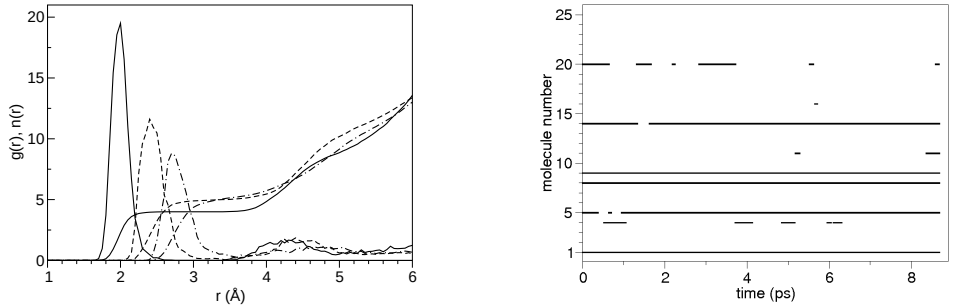

a) b)

Figure 2.5: a) Pair distribution functions and relative integration numbers for the $O\cdots M^+$ contacts; full lines: M=Li; dashed lines: M=Na; dotted-dashed lines: M=K. b) Life time for $O\cdots K^+$ contacts. Each line means how long a molecule remains inside the first minimum distance (3.80 Å) of the g(r) and belongs to the solvation shell. Molecules 1, 8 and 9 are always bonded (8.68 ps), molecules 14 and 5 are almost always bonded (8.37 ps and 8.18 ps, respectively), molecules 20, 4 and 11 have a short residence time (2.11 ps, 1.56 ps and 0.41 ps, respectively), and molecule 16 is bonded for only 0.06 ps. The average residence time is about 5.2 ps.

number as it is actually found and summarized in Tab. 2.1. The broadening and lowering of the first peak in the pair radial distribution functions going from Li^+ to Na^+ and K^+ are associated with a reduced strength of the interaction. The broadening of the first peak in the g(r) implies a higher possibility of penetration in the potential energy well and therefore a higher mobility of the solvent molecules.[162] In fact, as it can be recalled, the g(r) is related to the mean field potential,[163] giving an indirect information on the average strength of the interaction.

A more precise description of the mobility of the solvent cage is obtained considering the residence time of the solvent molecules in the first solvation shell. Li^+ and Na^+ interact with 4 and 5 molecules, respectively, in a stable way, and the molecules reside permanently in the solvation shell all along the simulation time.[48,89,164,165] The estimated lifetime of the molecules in the first solvation shell in the case of Na^+ is greater than 8 ps. In the case of K^+ the larger amplitude of motion is associated with a diffusion and an exchange of solvent molecules in the first and second solva-

tion shell. Fig. 2.5b identifies, as a function of time, the molecules bound to K^+ in the first solvation shell. A molecule is defined to belong to the first solvation shell if the distance of its oxygen atom from the K^+ ion is smaller than the first peak position in the g(r) function. It can be seen that molecules numbered 1, 8 and 9 are permanently in the shell, molecules 5 and 14 are almost constantly in the shell and other molecules alternate as first neighbours. The overall balance leads to a coordination number of 5.41. This can be attributed to the larger ionic radius of K^+ that allows, on average, a higher number of first neighbor solvent molecules.

A three-dimensional description of the motion of the Na^+ and K^+ ions around the solvent molecules is shown in Fig. 2.6, through the spatial distribution functions.[166–169] The isosurface close to the methanol molecule represents the probability to find the ion in a certain position, giving a clear view of the mobility of the solvation cage. As expected, at the same isosurface value (in our case each point has to be visited for 100 times), the K^+ ion spans a larger configurational phase space than the Na^+ ion.

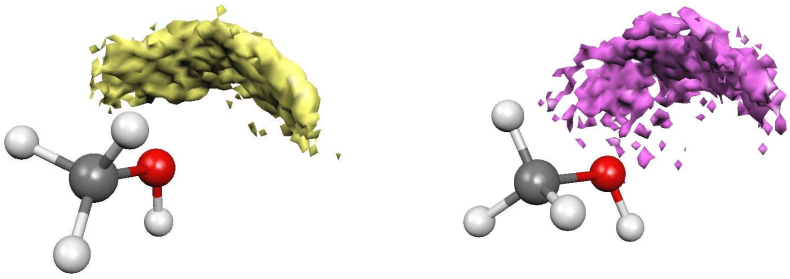

a) b)

Figure 2.6: Spatial distribution functions for Na^+ (a) and K^+ (b).

A picture of the electronic rearrangement in the solution is obtained from the calculation of the electric dipole moment of the first shell methanol molecules. The dipole moment has been obtained from the positions of the MLWF. The distribution of the dipole moment of the methanol molecules in the solution for the three ions is reported in Fig. 2.7a, Fig. 2.7b and Fig. 2.7c (for Li^+, Na^+ and K^+, respectively)

where the contributions of the whole solution and of the first solvation shell are compared. The average values of the dipole moment are summarized in Table 2.2.

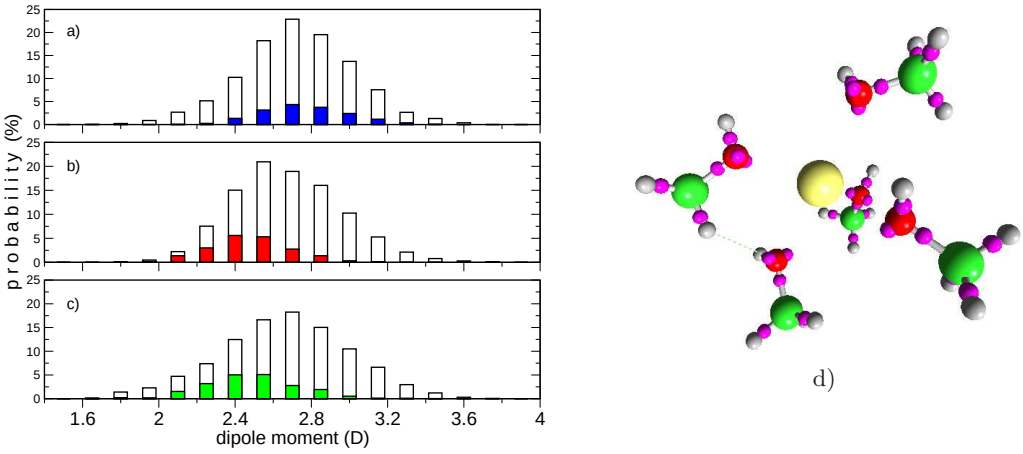

Figure 2.7: Dipole moment distribution (in debye, D) for: a) Li^+; b) Na^+; c) K^+. The coloured bars refer to the dipole moment distribution of the first solvation shell molecules. d) A snapshot of the WFCs for the first shell of Na^+.

	$< \mu >_{tot}$	$< \mu >_{fs}$
Li^+ (Pagliai *et al.*)[48]	2.73	2.76
Na^+	2.67 ± 0.28	2.48 ± 0.21
K^+	2.66 ± 0.34	2.49 ± 0.26

Table 2.2: Average dipole moment values (in debye, D) and relative standard deviation for the solution ($< \mu >_{tot}$) and for the first shell molecules contribution ($< \mu >_{fs}$).

In Na^+ and K^+ the distribution in the first solvation shell is $\sim$ 0.2 D lower than in the whole solution. This situation is quite different from that found for Li^+, where $< \mu >_{tot} \simeq < \mu >_{fs}$. As a whole the behaviours of Na^+ and K^+ are similar and the charge transfered to the ions are almost identical (-0.106 e^- for Na^+ and -0.108 e^- for K^+)[50] and approximately half the value found for Li^+ (-0.2 e^-).[48] Therefore, the solvent molecules in the solution of Na^+ and K^+ are much less polarized than in Li^+.

An interesting analysis of the charge redistribution in the solution can be obtained with the AIM method.[149–151] The results, as a function of the ion-oxygen distance, are reported in Fig. 2.8a and Fig. 2.8b for Na^+ and K^+, respectively. The behaviour is similar to that reported for the Na^+ and K^+ ions in water.[170]

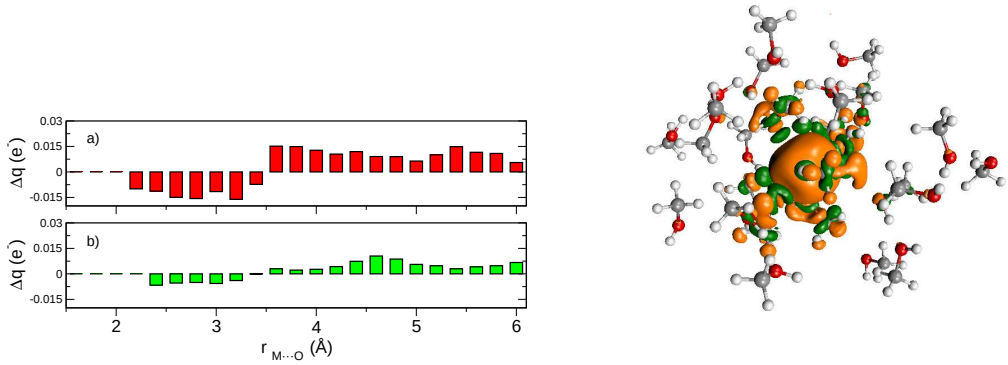

Figure 2.8: Transferred electronic charge distribution $\Delta q(e^-)$, as a function of the distance between the ion and the oxygen atom of methanol molecules $r_{M\cdots O}$. The reported values are integrated on a sphere. a) M=Na^+; b) M=K^+. The charge in the first solvation shell is -0.063 e^- and -0.057 e^- for Na^+ and K^+, respectively. The charge outside the first solvation shell amounts to 0.168 e^- and 0.163 e^- for Na^+ and K^+, respectively. The sum of this two terms balances the charge transferred to the ion with an uncertainty on the third decimal place. c) Electronic density flux for a selected configuration, The decrease and the increase in electronic density are reported in green and orange respectively.

The already discussed transfer of negative charge from the first shell molecules to the ions is more than counterbalanced by a charge transfer from the outer to the first shell molecules through the hydrogen bond network. As a net balance the positively charged ion is surrounded by a negatively charged first shell and a positively charged second shell. A qualitative view is confirmed by Fig.2.8c reporting the flux of electronic density.

This charge alternation contributes to the stability of the cage structure and a tighter reorganization of the solvent. The stability of the first solvation shell for Li^+

is enhanced by the larger charge transfer (-0.2 e^-).

2.2.2 Conclusions

Ab initio CPMD simulations have been performed on Na^+ and K^+ ions in liquid methanol to obtain several details on the structure and electronic properties of the first solvation shell. It has been shown that simple cations are strongly bound to the methanol molecules of the first solvation shell forming a stable cage, mainly for Na^+. AIM population analysis has shown that charge transfer from the first shell methanol molecules to the ions is more than balanced by the charge transfer from methanol molecules of the second shell such that the first solvation shell molecules are negatively charged. This contributes to stabilize the cage through electrostatic interactions. It has been confirmed that the methanol molecules in the first solvation shell are characterized by a preferred orientation with the lone pairs of the oxygen atom pointing toward the ion,[81,128] as reported in fig 2.7d for Na^+, but a similar behaviour occurs for K^+. The polarization of the solvent molecules has been studied through the WFCs analysis. The comparison with the pure solvent[34] emphasizes the perturbation due to the ions that is restricted to the range of the first solvation shell.[126]

2.3 Mg^{2+} and Ca^{2+}

Ab initio CPMD simulations have been performed in order to investigate the solvation properties of Mg^{2+} and Ca^{2+} in fully deuterated methanol solution[51] to better understand polarization effects induced by the presence of the ions. This kind of approach has been used with success to study ions in solution[48–50,117,160,161,171–180] showing that the most relevant contributions are concerned with the first solvation shell. The nature of the interactions that stabilize the first solvation shell of the Mg^{2+} and Ca^{2+} ions in methanol has been interpreted in terms of electronic contributions. Charge transfer and dipole moment investigations have been performed to give a detailed insight on the effects of the electronic reorganization on the stability of the solvation shell, confirming the stabilization model proposed in the case of the

Li^+,[48] Na^+ and K^+ ions[50] in the same solvent. The perturbation of the methanol H-bond network due to the ion has been also investigated. Problems arising from box side effects and sample size for highly charged systems have been taken into account performing simulations with two different box sides per ion, containing 25 or 40 solvent molecules, respectively.

2.3.1 Results

Samples with 25 methanol molecules have been initially simulated for both Mg^{2+} and Ca^{2+} ions.[51] In the case of the Mg^{2+} a peculiar behavior has been noticed with a fivefold coordination during the initial 7.3 ps of the run and a square pyramidal basis coordination geometry. Subsequently the number of methanol molecules around the ion rises up abruptly to a stable sixfold octahedral coordination. In order to explain this behavior, the energy of the optimized geometry for the two configurations (extracted before and after the coordination number change) has been computed for isolated clusters with "all electrons" calculations, using the BLYP functional and the 3-21+G** basis set. The results show a higher stability of the sixfold coordinated cluster with a difference in the binding energy of 29.95 kJ mol^{-1}. This value is about one order of magnitude higher than the thermal energy at 300 K (2.49 kJ mol^{-1}) and explains the observed stability of the sixfold coordinated ion once it is formed. The initial fivefold configuration can be attributed to the selected starting configuration and to a likely too short thermalization run ($\sim$ 1 ps) with respect to the cage relaxation time.

In Fig. 2.9 the pair radial distribution function g(r) for the Mg$\cdots$O and Ca$\cdots$O distances, together with their integration number, is reported for samples with 40 methanol molecules and compared with the system containing 25 solvent molecules.

It is evident that, for both ions, the sample dimension only affects the second solvation shell that is slightly better defined in the larger sample, showing clearly that it is formed by 6 molecules. A small effect on the height and width of the first peak can be noted in the case of $Ca^{2+}$for the smaller simulation box, implying a greater rigidity of the first solvation shell. The stability of the second shell is higher

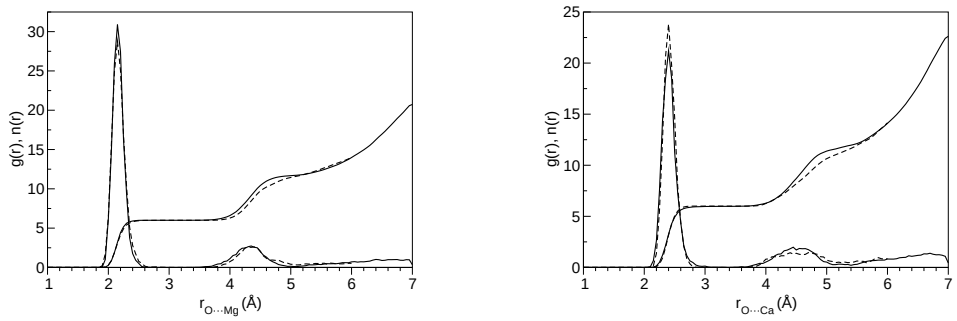

Figure 2.9: Pair radial distribution functions and integration numbers of Mg^{2+} (a) and Ca^{2+} (b) with 25 methanol molecules (dashed lines) and with 40 methanol molecules (full lines).

for the larger samples as it can be inferred from the slightly deeper second minimum.

Tab. 2.3 reports the position of the first peak in the radial distribution function and the integration number.

	$O\cdots M^{2+}$	cut-off	n(r)
Mg^{2+} (25)	2.15	3.00	5.6 (5 or 6)
Mg^{2+} (40)	2.15	3.00	6.0
Radnai *et al.*[181]	2.068		5.95
Tamura *et al.*[182]	2.00	2.5-3	6.0
Ca^{2+} (25)	2.40	3.25	6.0
Ca^{2+} (40)	2.40	3.45	6.0
Megyes et al.[183,184]	2.39		6.0

Table 2.3: Salient structural data (distances in Å) for Mg^{2+} and Ca^{2+} solutions with 25 and 40 solvent molecules. The coordination number, n(r), has been computed at the cut-off distance in the minimum of the distribution functions. The data are compared with experimental results.

It can be seen that the cut-off distance has no effect on the coordination number due to the fact that the first minimum in the g(r) is widespread. X-ray diffraction studies[181] locate the first peak position at 2.068 Å with a "relatively rigid octahe-

dral" cage thus proposing a sixfold coordination. Subsequent studies, supported by molecular dynamics simulations,[182] confirmed these findings although with a first peak position at shorter distance (2.00 Å) than the X-ray result. In the present calculation the first peak position for Mg^{2+} solutions is found at slightly larger distance (2.15 Å). The results of the present simulation are in full agreement with experiments[183,184] in the case of the Ca^{2+} ion.

For both ions the residence time of the methanol molecules in the first solvation shell is longer than the simulation time and no exchange of methanol molecules has been observed between the first and second solvation shell, as can also be argued by the flat and deep minimum in the pair radial distribution functions. A similar behavior has been reported for water solution where many of these ions are surrounded by a rigid first solvation shell that shows a slow exchange of water molecules with the second shell.[58,101,153,185,186] Earlier, diffusion coefficient calculations from solvation simulations reported a very long life time for water molecules in the first solvation shell around Mg^{2+}, falling in the range of hundreds of picoseconds.[187,188]

The small amplitude of motion in the cage is well evident from the pair distribution functions (Fig. 2.9) characterized by a very sharp first peak. This is further emphasized by the spatial distribution functions[166–169] of Fig. 2.10 where a pictorial view of the first solvation shell is dislayed together with the motion amplitude of the oxygen atoms around the ion. The spanned configurational space is found to be strictly localized around the vertices of an octahedron, particularly for Mg^{2+}, as can also be argued from the lower dispersion of the data.

The perturbation on the solvent structure, due to the presence of the ion, has been evaluated in terms of electronic properties that illustrate the differences from the pure solvent.[34] The polarization effects are highlighted by the dipole moment computed through the MLWF and shown in Fig. 2.11.

The ion perturbation mainly affects the neighboring molecules that are highly polarized as it is seen from the change of the average total dipole moment ($\Delta\mu \sim 0.4$ D). In turn the dipole moment of the outer molecules approaches to the value of the pure liquid (2.6 D)[34] remarking the weaker perturbation at long range. These re-

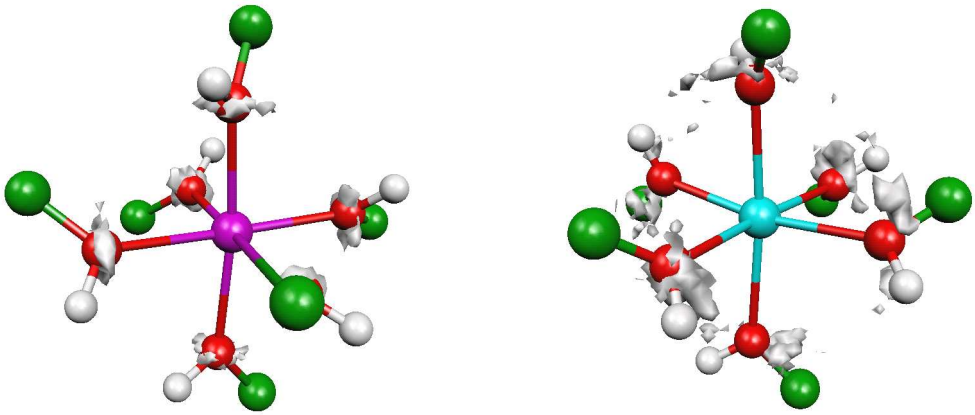

a) b)

Figure 2.10: Spatial distribution functions for the first solvation shell of Mg^{2+} (a) and Ca^{2+} (b) in the system with 40 methanol molecules. The isosurface represents the 13% and the 16% of the maximum value for Mg^{2+} and Ca^{2+}, respectively. The methyl groups have been represented by the green spheres for clearness.

sults are summarized in Tab. 2.4 where it can be noted that the contribution to the dipole moment does not depend on the system size. The polarization provided by monovalent cations on the surrounding methanol molecules was found weaker as reported for Na^+ and K^+ (Sec. 2.2 from Pag. 15). The stronger polarization due to these alkaline-earth ions with respect to alkaline ions has been also reported in water solution.[180]

	$< \mu >_{tot}$	$< \mu >_{fs}$	$< \mu >_{ext}$
Mg^{2+} 25	2.9 ± 0.4	3.4 ± 0.4	2.7 ± 0.3
Mg^{2+} 40	2.8 ± 0.4	3.3 ± 0.2	2.7 ± 0.3
Ca^{2+} 25	2.8 ± 0.4	3.2 ± 0.3	2.7 ± 0.3
Ca^{2+} 40	2.8 ± 0.4	3.3 ± 0.3	2.7 ± 0.4

Table 2.4: Average dipole moment values (in debye, D) and relative standard deviation for the solution ($< \mu >_{tot}$), for the first shell molecules contribution ($< \mu >_{fs}$) and for the external molecules ($< \mu >_{ext}$).

For alkaline ions the size of the ions increases going from Li^+ to K^+ and conse-

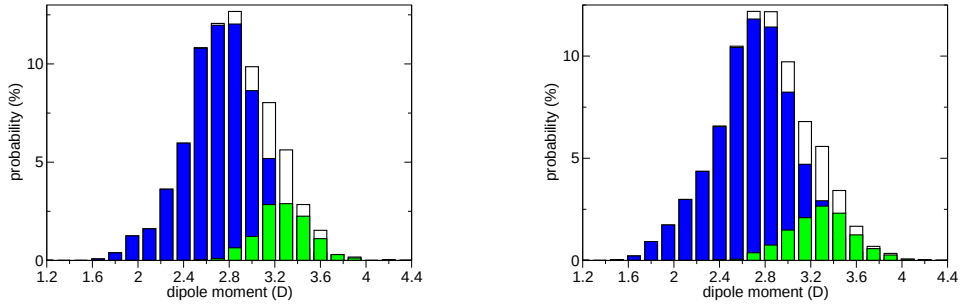

Figure 2.11: Dipole moment for methanol molecules with Mg^{2+} (a) and Ca^{2+} (b). The green bars refer to the dipole moment of the first shell molecules, whereas the blue bars describe the external molecules contribution. The average dipole moment of the whole solution is represented by the white bars.

quently, as expected, the induced dipole moment of the solvent molecules decreases. This is particularly evident for the first solvation shell molecules.[50] For magnesium and calcium ions a different trend can be observed: the longer O-Ca distance does not yield a weaker polarization effect with respect to magnesium ion and the perturbation on the dipole moment values is similar for both ions.

Radial $r_{O\cdots W}$ and angular $\theta_{W\cdots O\cdots W}$ distributions of the WFCs of the oxygen lone pairs have been investigated to better understand the increase of the dipole moment of the first solvation shell molecules.[189] These are reported in Fig. 2.12 showing separately the contribution of the first solvation shell molecules.

A different shape in the distribution of the $r_{O\cdots W}$ distances and a lower value in the $\theta_{W\cdots O\cdots W}$ angles are observed for the first shell molecules, whereas no change occurs between the oxygen and the WFCs attributed to the O-H and O-C covalent bonds (not reported). For the $\theta_{W\cdots O\cdots W}$ angle a smaller value can be observed for the lone-pair WFCs of the first shell molecules both in methanol and water solution,[171,173,189,190] while a different behavior is present in the $r_{O\cdots W}$ distance in the two solvents. A double peak in the distribution of $r_{O\cdots W}$ is found for the external molecules in methanol, while a symmetrical distribution has been found for

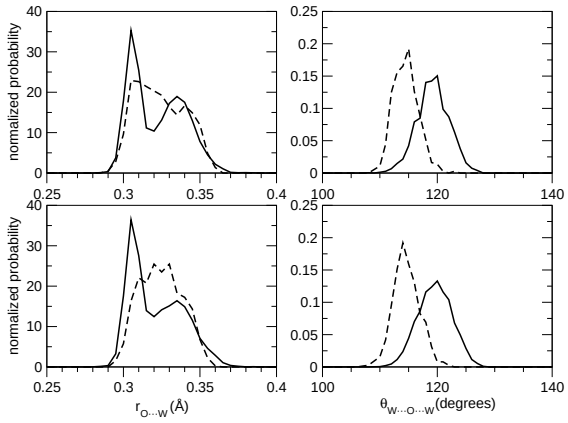

Figure 2.12: Radial distribution function of the oxygen-WFCs average distance ($r_{O\cdots W}$) and angular distribution function of the angle between the WFCs ($\theta_{W\cdots O\cdots W}$) for Mg^{2+} with 40 methanol molecules (top) and for Ca^{2+} with 40 methanol molecules (bottom). The dashed lines refer to the first shell molecules contribution.

the molecules directly solvating the ion. In the bulk, where no coordinative constrain is imposed, some methanol molecules are directionally H-bonded[34] through a single WFC. The methanol H-bonded lone-pairs are less contracted on the oxygen than the non-interacting lone-pairs providing a splitting of the peak. No H-bond network is permitted between the molecules of the first solvation shell. This can be attributed to the steric hindrance of the CH_3 group. The first shell methanol molecules interact with the ion through both the WFCs that are therefore not anymore available to accept hydrogen atoms from other methanol molecules.

A further insight on the solvent reorganization produced by the ion is obtained considering the angle θ_μ between the dipole moment vector ($\vec{\mu}$) and the oxygen-ion interaction axis as depicted in Fig. 2.13.[182,191]

For the first shell molecules it can be seen that θ_μ is quite tightly peaked around 18 °, indicating a rigid structure of the solvation shell. For the outer molecules the distribution is very shallow. A similar behaviour has been generally observed in

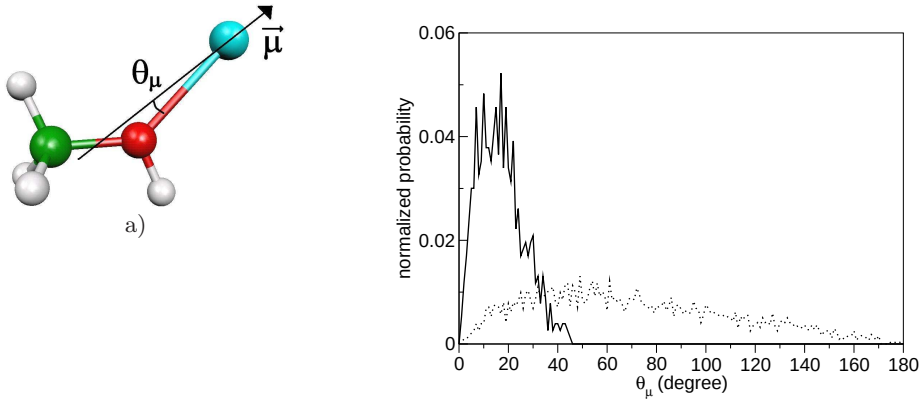

Figure 2.13: a) Definition of the θ_μ angle between the dipole vector ($\vec{\mu}$) direction on the methanol molecules and the Ca-O axis. b) Distribution function of θ_μ for the system with 40 molecules. The full line refers to the first shell contribution. The dotted line represents all other external molecules.

water solutions[19,21,118,160,161,180,192] and only rarely in other solvents.[88]

This behaviour can be further enlightened considering the variation of the dipole moment orientation as a function of the distance from the central ion as reported in Fig. 2.14a.[19,182,191,192]

Neglecting the 3-4 Å range, where the statistics is rather poor, it can be seen that, up to 5 Å, θ_μ increases smoothly and the deviations from the average value are small implying that there is a preferential orientation of the dipoles in the first and even in the second shell. Above 5 Å a higher disorder in the bulk of the solution is evident. Similar results have been obtained for Mg^{2+}.

The charge transfer analysis on the ions has been performed using the AIM approach proposed by Bader.[149–151] This method allows to evaluate the amount of the charge transfer as a function of the distance between the ion and the surrounding solvent molecules as it is depicted in Fig. 2.14b for Mg^{2+} with 40 methanol molecules. The electronic charge transfer on the ions is 0.221 ± 0.003 e^- for Mg^{2+} and 0.347 ± 0.008 e^- for Ca^{2+}. The same trend was also observed in water solutions.[180] A smaller electronic displacement was noticed for alkali metal cations to-

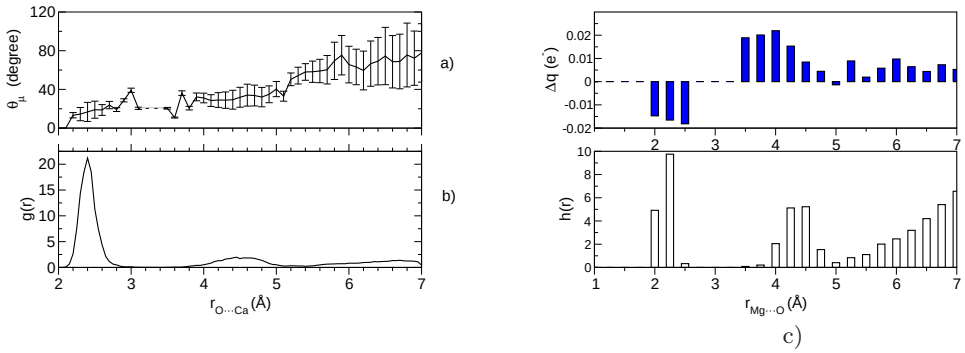

Figure 2.14: a) Standard deviation on the average value of the θ_μ angle as a function of the distance from Ca^{2+} in the system with 40 methanol molecules. b) O-Ca pair distribution function (same as Fig. 2.9b with full lines). c) Charge transfer distribution $\Delta q(e^-)$ as a function of the distance to the ion (upper panel) and not normalized O-Mg distribution function (lower panel) for Mg^{2+} with 40 methanol molecules.

gether with a weaker polarization effect on the first shell molecules.[48,50] The higher value for the calcium ion is due to the greater softness with respect to the magnesium ion as expected in going down along the group in the periodic table.[193] The same number of valence shell electrons and the same charge on Mg^{2+} and Ca^{2+} are distributed in a different atomic volume. The higher ionic radius[162,194] of Ca^{2+} implies a difference in hardness,[195,196] namely the resistance of the chemical potential to change the number of electrons.[193] Ca^{2+} can receive a greater charge amount from the first shell molecules that become very positively charged. The charge transfer from the second shell to the first is not sufficient to balance the charge transferred from the methanol molecules of the first solvation shell to the ion.

2.3.2 Conclusions

Ab initio CPMD calculations have been performed on solutions of methanol with Mg^{2+} and Ca^{2+} in order to investigate the reorganization effects on a protic solvent due to the presence of charged species. Distribution functions, AIM population analysis and MLWF has been adopted to investigate the first solvation shell properties

compared to the bulk solvent molecules either from a structural and electronical point of view. The box size effects have been explored and no evident consequence has been found on the first solvation shell. Similar structural and electronic reorganization is induced on the solvent by the two ions. A stable octahedral coordination and a high polarization effect on the molecules of the first solvation shell have been observed. Analysis of the dipole moment vector has shown a preferential orientation up to 5 Å far from the Ca^{2+} slighly affecting the organization of the second shell as well. The characterization of the hydrogen bond network through the distribution functions of the WFCs has shown a different trend with respect to that observed in water solution[171,173,189,190] without any solvent molecule in the first solvation shell behaving as a H-bond acceptor. Electronic charge transfer analysis has confirmed the stabilization of the first solvation shell due to electrostatic interactions.

3

Parallelization of a code for Bader analysis

During the last few years computational and numerical methods have turned out to be very worthy and useful for the progress in the scientific research and nowadays, by characterizing a system through first principles studies, they have been widely exploited in order to foresee the behaviour of a large number of chemical-physical systems. In particular, computational chemistry has become an important investigation tool able to confirm and explain a huge variety of experimental data and to obtain results often hard to achieve with the modern laboratory instruments.

Through the Car-Parrinello Molecular Dynamics (CPMD) simulations within the density functional theory formalism it is possible to follow the electronic structure evolution of a system providing an accurate description of the interactions coming out between the involved species. An important characteristic to be considered in a simulation deals with the charge placement on atoms because variations in the charge distribution may affect significant properties of a system.

Some years ago, Richard F. W. Bader suggested an intuitive method to share electrons in an appropriate way inside a molecular context.[150,151] Density charge has a minimum between the atomic species and may result a direct method to distinguish different atoms. The Bader volume describes the space limited by zero-flux

surfaces. In particular the charge density turns out to be a perpendicular minimum upon these surfaces. Starting from the definition for which an atom is entirely described by its electronic charge, the total charge wrapped in the Bader volume is a good approximation of the charge present upon an atom. The theory of Atoms in Molecules, according to the decomposition in Bader volumes, allow to accurately assign the total charge upon every atom. Through the charge distribution it is possible to determine interesting electronic properties such as multipole moments that may become fundamental parameters to explain the interactions between atoms and to describe the correct behaviour for a wide variety of chemical systems.

The plenty of data obtained from a molecular dynamics simulation is often very huge. In order to have statistically significant results on the charge distribution, a great number of configurations should be extracted from a trajectory, with a long computational time required for the subsequent interpretations.

During the years A. Arnaldsson and G. Henkelman have developed and improved an algorithm[149] to separate the single atomic contribution from the total density charge in a molecular system, exploiting the methodology proposed by Bader.[142,145,148] The algorithm reads charge distributions in a *.cube* file format, scaling linearly with the number of grid points.[142,148] It can be applied to large system because the scalability does not depend on the number of atoms or on the interaction topology.[142] The adoption of a massive parallelization of the program will considerably reduce the computational time, mainly for those systems which need an analysis on a great number of configurations. Moreover it will be possible to study variations on the charge values as a function of simple variables, such as the mesh spacing of the grid, to see how they are influenced with a little overall time waste.

For this purpose the *FORTRAN* algorithm proposed by Arnaldsson *et al.*[149] has been implemented with the use of *MPI* libraries for the high performance parallel computation. The parallelization strategy for the charge computation on the atoms has been based on distribution of the configurations over the processors with a *Master-Slave* approach. The Master processor arranges on the $n-1$ Slave processors

the configuration files in a way that they are contemporaneously processed. Then the Master puts itself on listening in order to receive informations from the slave processes as soon as they are free of computational load. The global computation will halt when all the Slave processors has sent the stop message. This setting is highly portable to those system for which it is permitted to process contemporaneously many independent files in order to make the highest scalability of such an approach. The resources used to perform computations and tests are located at CINECA, University Consortium.[197] The hardware, named BCX (1280 nodes Blade LS21 - 2 AMD Opteron(tm) Processor 2216 HE dual-core 2.4 GHz 10240 GB RAM) and SP5 (512 POWER 5 1.9 GHz CPU 1216 GB RAM), has been made available to build the parallelization of the algorithm and to execute the following tests.

3.1 Results

A system made up by 256 files *.cube* with a 216^3 grid points (25729 KB for every file) has been taken into account. The configurations have been extracted from a CPMD simulation to describe to solvation dynamics of a molecule of 1,1,1,3,3,3-hexafluoroisopropanol (HFIP) in water solution.

One of the configurations obtained from the CPMD simulation is depicted in Figure 3.1. The cubic cell with a side of 11.34 Å is composed by one molecule of HFIP surronded by 40 solvent molecules, for a total of 132 atoms.

In order to evaluate the scalability of the algorithm, an increasing number of processors has been used on both platforms made available by CINECA. In Figure 3.2a the execution time has been plotted as a function of the number of processors. An exponential descrease in the execution times can be noticed up to 64 processors, value at which the best performance has been obtained on BCX. A poor improvement in the comuptational time is noticed on SP5 over 64 processors and it is not convenient to use further hardware resources. This is probably due to the saturation concerning the I/O.

The serial algorithm takes 2085 s and 2239 s on BCX and SP5, respectively, to

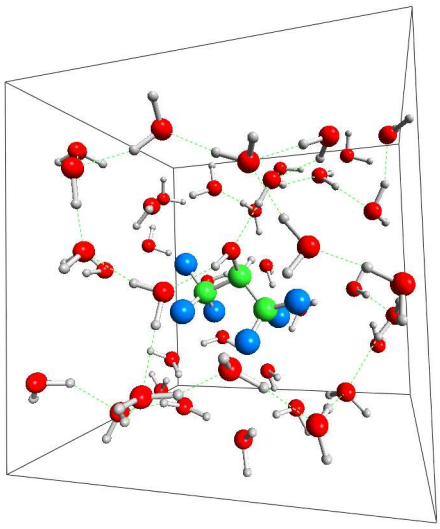

Figure 3.1: Configuration extracted from the CPMD simulation. The box contains one molecule of HFIP and 40 water molecules.

process 256 configurations. Even if this time may depend on the average load on the machines, a neat improvement on the computational time up to ~ 100 times is evident as reported in Tab. 3.1.

A series of computations have been performed in order to assure the reproducibility of the results obtained and to take into account the influence of the computational load present on the machines at the moment of the measurements. On this purpose, 4 and 16 processors have been used on BCX, whereas tests with 8 and 32 processors involved SP5. For everyone of these four systems, 12 computations have been performed, erasing subsequently the best and the worst time recorded. The average time and the standard deviation on the results have been plotted in Fig. 3.2b on every series of measurements. The standard deviations put in evidence tiny variations on the average times. More relevant differences can be noticed when the number of processor is smaller (for BCX 4 and SP5 8) where the execution time is higher as the influences deriving from a supplementary computational load on the machines.

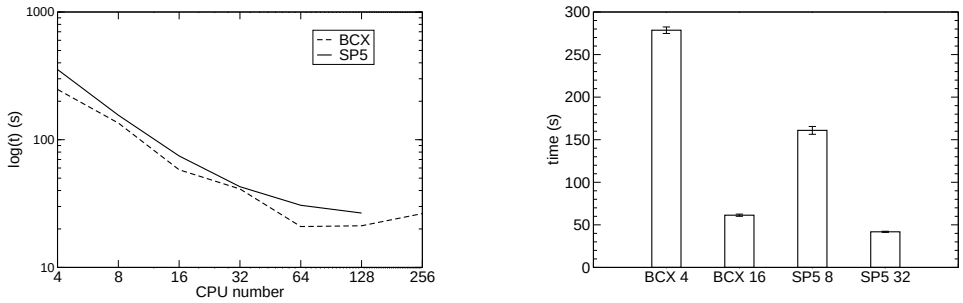

a) b)

Figure 3.2: a) Execution time (in seconds) of the algorithm as a function of the number of the processors on the platform BCX and SP5. Logarithmic scale has been adopted on Y-axis to put in evidence the linear scalability of the system. b) Computational time histogram (in seconds) and relative standard deviation. On BCX, 4 and 16 processors have been used (BCX 4 and BCX 16, respectively), whereas 8 and 32 processors have been used on SP5 (SP5 8 and SP5 32, respectively).

3.2 Conclusions

At CINECA Computational Center an efficient parallelization strategy of the type *Master-Slave* on a serial algorithm for the Bader charge analysis has been set up in order to give a more efficient elaboration of a great amount of data and to accelerate the interpretation of the subsequent results. A remarkable increment of the performance has been obtained up to 64 processors and a computational time by ~ 100 times faster with respect to the serial algorithm has been achieved. From a wider point of view, this methodology may be correctly extended to a series of applications which can exploit this kind of parallelization to improve the efficency of the time to obtain results. In general this can be important when it is necessary to study the influence of some parameters on the accuracy of the final results because the setting of the initial variables may involve the redundant repetition of the computations. The optimal scalability of the method allows to obtain results even with a reduced computational resource. With the use of only 8 processors, the performance may improve over 15 times with respect to the serial algorithm as can be proved by the

# CPUs	BCX	SP5
serial	2085	2238
4	247.39	354.50
8	135.04	155.58
16	58.15	74.64
32	41.14	42.86
48	40.91	35.33
64	20.89	30.66
72	21.92	28.04
128	21.18	26.65
256	26.41	—

Table 3.1: Execution time of the algorithm (in seconds) either for BCX and SP5 platform as a function of the number of processors.

algorithm execution times reported in Tab. 3.1.

4

Fluorinated alcohols as stabilizing cosolvents

Fluorinated alcohols are increasingly applied in conformational studies of biochemical systems due to their secondary structure stabilization properties,[198–210] especially α-helix, and capability to mimic the cell environment.

In order to obtain a deep knowledge about the stabilization mechanism and interactions between fluorinated alcohols and proteins or peptides, experiments and computational findings have been applied to analyze the chemical species that have been found particular by promising for this purpose. The most studied fluorinated solvents are 2,2,2-trifluoroethanol,[200–203,205,210–214] 1,1,1,3,3,3-hexafluoroisopropanol (HFIP)[208,209,215–218] and 1,1,1,3,3,3-hexafluoroacetone (HFA).[204,207,219–221] Although these studies have not clarified the interactions leading to the secondary structure stabilization when fluorinated alcohols are used as cosolvents in water solution, a series of hypothesis have been formulated to explain this behavior. It has been observed[214,222,223] that these alcohols form clusters with an inner hydrophobic core, whereas the OH groups interact with the water molecules, giving rise to micelle-like structures. Experiments on fluorinated alcohol/water mixtures showed a maximum aggregation around 30% (v/v) for HFIP.[215,222] The hydrophobic interactions between CF_3 groups and the protein side-chains hinder water molecules from forming

or breaking H-bonds of the protein. The cosolvent coats the protein, avoiding water molecules to interact with the internal C=O$\cdots$H-N H-bonds between aminoacid residues[206,213] and to destabilize the backbone conformation.

A systematic study has been performed starting from the analysis of the interaction of HFIP and HFA with water by *ab initio* molecular dynamics simulations within the Car-Parrinello method in order to obtain a further insight at the atomic level on the protein structural stabilization effects due to the fluorinated alcohols. Car-Parrinello Molecular Dynamics (CPMD) simulations allow a complete description of multi-body systems and polarization effects providing a powerful tool for the characterization of H-bonded interacting systems. This method correctly reproduces both structural, dynamic and spectroscopic properties.

The results of CPMD simulations of one molecule of HFIP in water solution have been adopted as a guide to validate a new developed semi-empirical potential model. This potential has been found capable to accurately reproduced the HFIP/water interaction and has been adopted to perform classical Molecular Dynamics (MD) simulations on fluorinated alcohol/water mixtures. A series of MD simulations on samples with different HFIP molar fraction (χ_{HFIP} = 0.020, 0.082 and 0.400) have been carried out, showing a good agreement between the theoretical results and the experimental available properties, such as structural parameters, diffusion coefficients and dielectric constants. A subsequent classical MD simulation of Melittin in ordinary HFIP/water solution has been performed to prove the effective stabilization role of such alcohol/water mixtures on the secondary structure of short polypeptides. These results represent the starting point to understand the stabilization effects of these cosolvents at a molecular level.

4.1 Simulation details

All the *ab initio* simulations have been performed with the CPMD code[9,10] in a cubic box with one molecule of HFIP or HFA and 40 water molecules with periodic boundary conditions at the density of pure deuterated water. A preliminary ther-

malization at 300 K by velocity scaling has been carried out. The simulations have been performed in the NVE ensemble for a total run of more than 16 ps for HFIP and over 32 ps for HFA. Deuterium has been used instead of hydrogen to allow for a larger time-step. Density functional calculations in the generalized gradient approximation have been performed using the BLYP[224,225] exchange correlational functional and Goedecker type pseudopotentials[226,227] have been used for all the atomic species. The plane wave expansion has been truncated at 85 Ry.[122] A fictitious electronic mass of 800 a.u. has been adopted to keep the system on the Born-Oppenheimer surface. The dipole moment values deriving from the CPMD simulations have been computed from the Wannier Function Centers (WFCs).

The classical MD simulation of the peptide Melittin (MLT) in explicit solvent has been performed using an in-house version of the program ORAC[228] and the Amber03[229] force field with TIP3P water.[107] The crystal structure of the complex of MLT (PDB code: 2MLT[230–232]) has been obtained from the Brookhaven Protein Data Bank[233] and it has been solvated by 186 HFIP molecules and 2091 water molecules in a cubic box with periodic boundary conditions in order to achieve the HFIP molar fraction of $\chi_{\mathrm{HFIP}} = 0.082$. The protein has been initially freezed and the solvent system has been thermalized by velocity scaling at T = 300 K and P = 1 atm. Subsequently a free dynamics of 1 ns has been accomplished for the protein relaxation. Afterwards the NPT simulation has been performed by integrating the equations of motion for 50 ns. The constant pressure has been obtained using a modification of the Parrinello-Rahman Lagrangian[234] and the temperature control has been achieved using a Nosé thermostat[235] with a mass of 30 cm^{-1}. The barostat[236] has been set up with an external pressure of 0.1 MPa (atmospheric pressure) and a mass of 60 cm^{-1}.

4.2 Hexafluoroisopropanol results

The HFIP molecule adopts two different conformations, antiperiplanar (*ap*) and synclinal (*sc*) that differ for the value of the H-C-O-H torsional angle (∼180° and

~30°, respectively), as can be observed in Fig. 4.1.

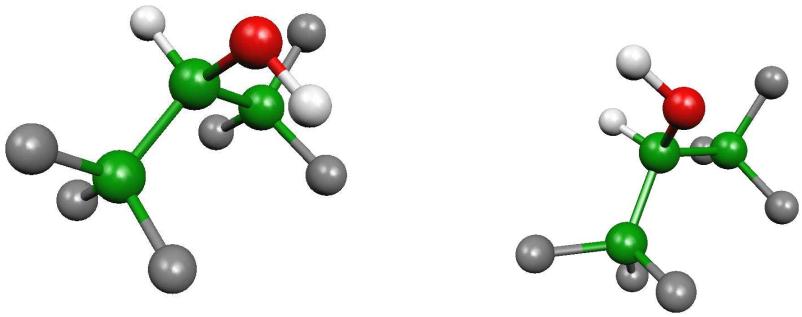

a) b)

Figure 4.1: Representation of the a) antiperiplanar (*ap*) and b) synclinal (*sc*) conformers of HFIP.

Recent high level *ab initio* calculations have shown that the two conformers are almost isoenergetic,[216,223,237,238] with the energy difference below 10 kJ mol^{-1} with the *ap* species at lower energy. It has been recently observed that the two conformers are still present both in CCl_4 and in water solutions.[237,239] In particular, relations between HFIP concentration and relative population of the two conformers in aqueous solution have been lately asserted.[239] On the basis of these experimental findings two different series of CPMD simulations have been performed on the *ap* and *sc* conformers in water. No conformational transitions have been observed during the two simulations. As a consequence in the following the structural properties of the two sample have been separately analyzed in terms of interactions with water, in particular H-bond, comparing the CPMD results with the most recent experimental findings.[240]

In order to analyze the interactions between HFIP and water, the pair radial and angular distribution functions involving HFIP/water H-bonds are reported in Fig. 4.2.

Taking into account the $H_{HFIP} \cdots O$ interaction (upper panels of Fig. 4.2), it is possible to note that the two conformers form a quite strong H-bond with water.

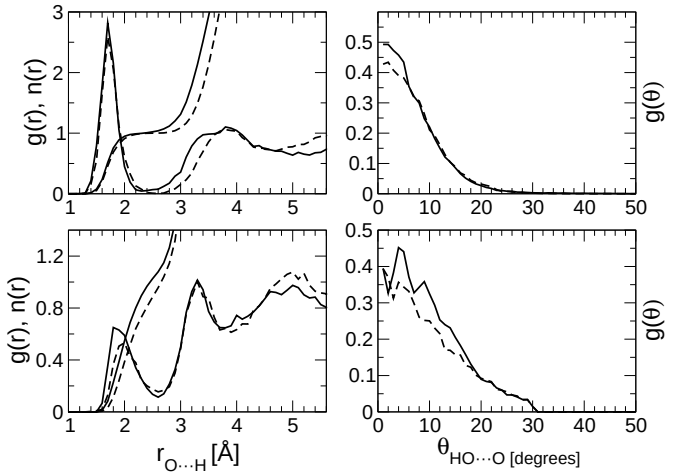

Figure 4.2: Upper panel: pair radial (left) and angular (right) distribution function for the $H_{HFIP}\cdots O$ interaction. Lower panel: pair radial (left) and angular (right) distribution function for the $H\cdots O_{HFIP}$ interaction. The full and dashed lines refer to the *sc* and *ap* conformers, respectively.

The interaction between the *ap* conformer and the first solvation shell molecules is stronger than the same interaction of *sc* species, even if the latter gives rise to a more extended interaction with a clearly defined second solvation shell. Otherwise, the strength of the HFIP/water interactions is higher for the *sc* conformer with respect to the *ap* one when considering HFIP molecule as acceptor of H-bonds (lower panels of Fig. 4.2). The directional character of the H-bond between HFIP and water is similar to that observed for other systems, like methanol[34] or water,[111] with a distribution that extends up to $\sim 30^{\circ}$.

A more detailed description of the H-bond configurational space can be obtained through the weighted radial-angular distribution functions,[34,49] $g(r,\theta)$, of Fig. 4.3 and the Spatial Distribution Functions (SDFs)[166–169] of Fig. 4.4.

It is interesting to note that the $g(r,\theta)$ functions confirm the trend in the strength of the H-bond previously observed in the distribution functions of Fig. 4.2. In this respect, the upper panels of Fig. 4.3 shows that HFIP in the *ap* conformer gives

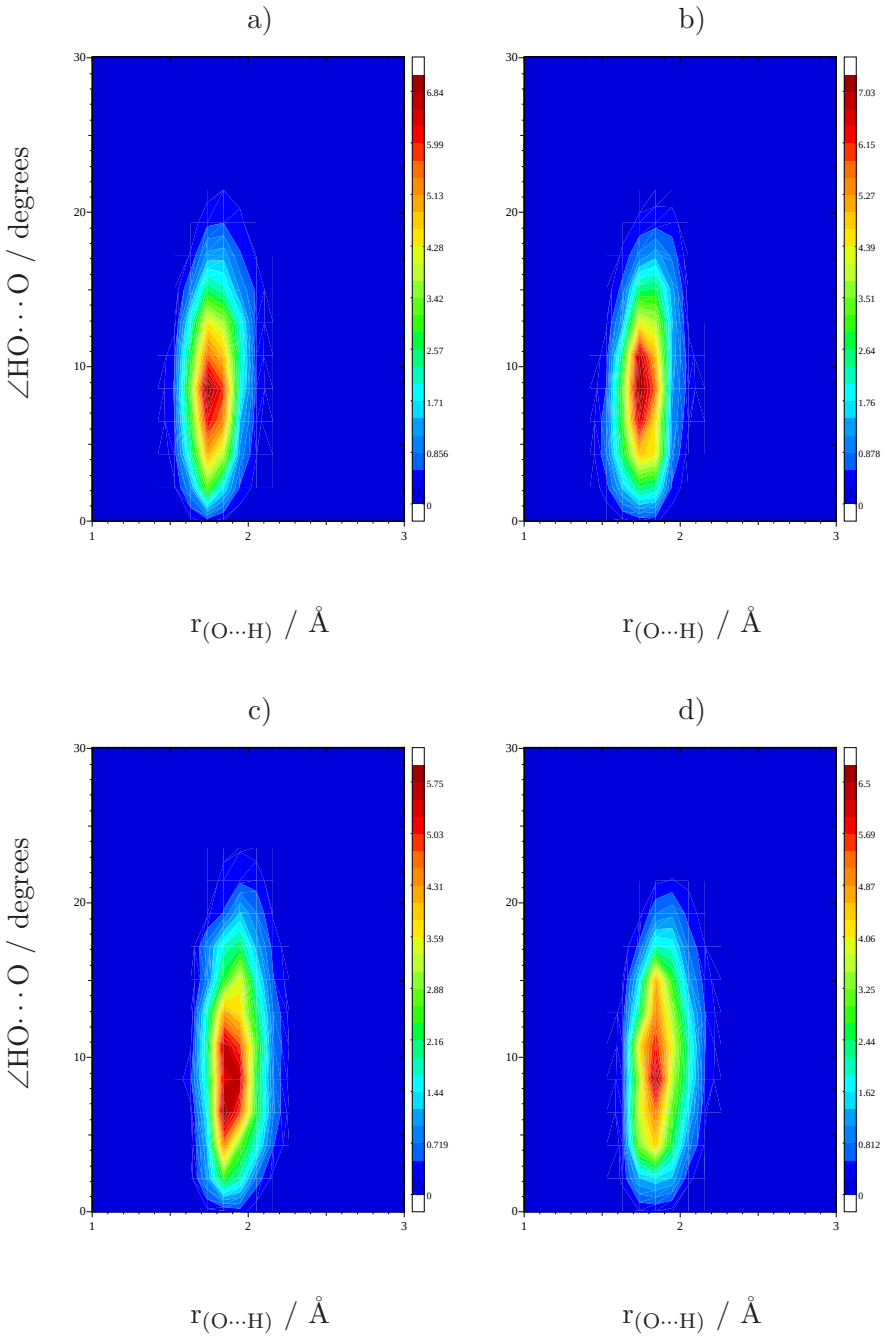

Figure 4.3: H-bond configurational space obtained as weighted g(r,θ) function. a) and c) surfaces are related to the $H_{HFIP} \cdots O$ and $O_{HFIP} \cdots H$ of the *ap* conformer, respectively; b) and d) surfaces are related to the $H_{HFIP} \cdots O$ and $O_{HFIP} \cdots H$ of the *sc* conformer, respectively.

rise to a strong H-bond with water that is characterized by low mobility, whereas the configurational space spanned by the *sc* conformer in the strong H-bond region is wider. The mobility of the H-bond in the region spanned by HFIP as acceptor is more similar for the two conformers, although a reverse behavior can be observed in this case (lower panels of Fig. 4.3).

A tridimensional picture of the H-bond configurational space that further confirms the behavior of HFIP in aqueous solution is reported in Fig. 4.4, where the SDFs are reported for the $H_{HFIP} \cdots O$ and $O_{HFIP} \cdots H$ contacts.

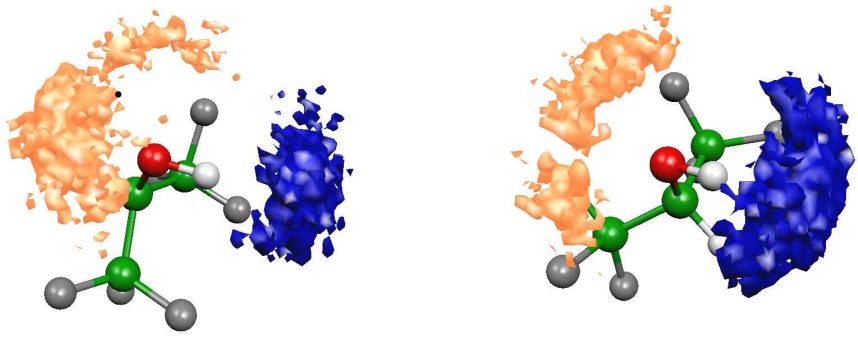

a) b)

Figure 4.4: SDFs for the a) *ap* and b) *sc* conformers; the blue and orange surface refer to the $H_{HFIP} \cdots O$ and $O_{HFIP} \cdots H$, respectively.

Since the HFIP solvent has been revealed particularly effective in the interactions with biological systems to stabilize α-helical structures, it is important to develop suitable force field for classical MD methods. In this respect, classical MD simulations have been initially performed with the description of the solute-solvent interactions through the new force field and the salient parameters are summarized in Tab. 4.1.

The necessary computational details for the samples have been retrieved from the CPMD simulations for a direct comparison of the results. The first insights on the quality of the new potential have been obtained comparing the main features of the pair radial distribution functions, reported in Fig. 4.5, with those obtained

atom	atom type	charge e^-
C_F	ct	0.415698
F	f	-0.142701
C_c	ct	-0.106031
H	h3	0.206203
O	oh	-0.471136
HO	hh	0.395774
bond type	force constant	distance (Å)
ow hw	553.00	0.9572
hw hw	553.00	1.5136
osp hsp	553.00	1.000
hsp hsp	553.0	1.633
ct h3	340.00	1.100
ct ct	310.00	1.55
ct f	367.00	1.380
ct oh	320.00	1.410
bending type	force constant	angle (degrees)
ct ct ct	40.00	109.50
ct ct oh	50.00	109.50
ct ct h3	50.00	109.50
h3 ct oh	50.00	108.50
f ct f	77.00	109.10
f ct ct	50.00	109.50
ct oh hh	55.00	108.50
torsion type	force constant	periodicity
x ct ct x	-0.1556	3
hh oh ct ct	0.0	1
hh oh ct h3	1.2856	1
hh oh ct h3	0.7396	2
hh oh ct h3	-0.6155	3

Table 4.1: Force field parameters. C_F is the carbon atoms of the CF_3 groups; C_c is the central carbon; HO is the hydrogen of the OH group; H is the hydrogen bound to C_c. The stretching force constants are in Kcal mol^{-1} $Å^{-2}$. The bending interactions are in Kcal mol^{-1} rad^{-2}. The torsional are in Kcal mol^{-1} and the periodicity means the number of minima (maxima) for 360 degrees rotation around the torsional axis.

during the CPMD simulations, showing a highly satisfactory agreement.

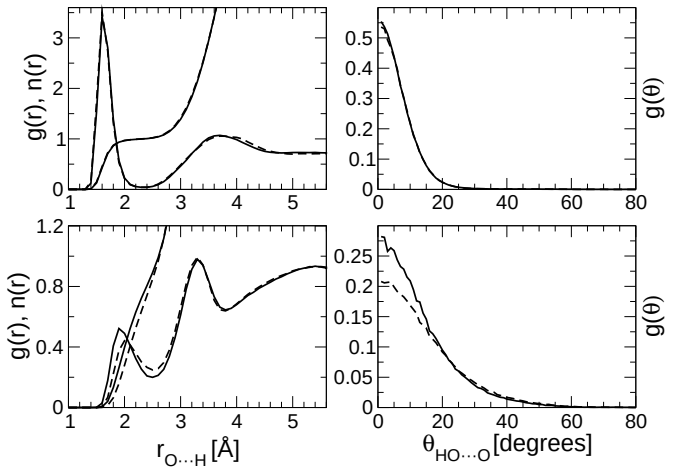

Figure 4.5: Pair radial and angular distribution functions for HFIP in spc/e (full line) and tip3/p water (dashed line). The upper and lower panels refer to the $H_{HFIP} \cdots O$ and $O_{HFIP} \cdots H$ interactions, respectively.

For the water molecules two of the most adopted potentials, tip3p and spc/e, have been used without observing significant differences in the two classical simulations for the acceptor and donor H-bond interactions.

For the classical calculations, the distinction of the *ap* and *sc* conformers is more difficult because several conformation interchanges occur during the run. This behavior is further clarified in Fig. 4.6a, showing the population distribution as a function of the dihedral angle $\phi_{H-C-O-H}$ adopting either the tip3p or spc/e potential. This situation can be rationalized on the basis of the low free energy barrier between the two conformers. The barrier height is $\sim$12 kJ mol^{-1}, allowing a rapid conformational interchange at room temperature. This change has not been noted in the CPMD simulations because of the shorter time explored by the phase space with respect to the average life time of a single conformation observed in the classical simulations.

To further validate the developed potential, a series of classical molecular dynam-

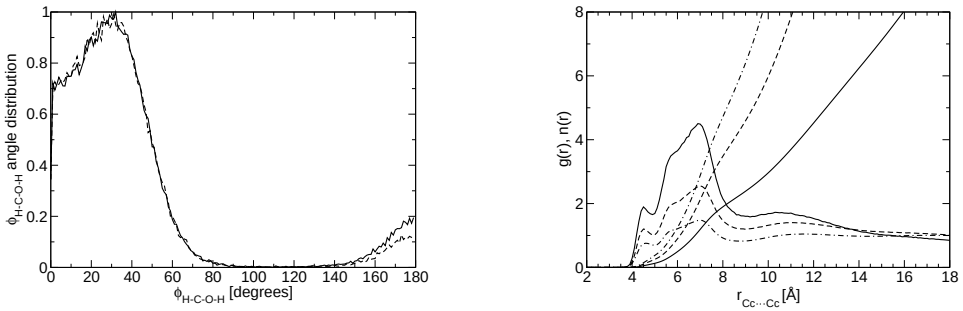

a) b)

Figure 4.6: a) Torsional angle $\phi_{\mathrm{H-C-O-H}}$ distribution (in degrees) for spc/e (full line) and tip3p (dashed line) model of water; b) Pair radial distribution function for the $C_c \cdots C_c$ interaction at the molar fraction χ_{HFIP}=0.020 (full line), 0.082 (dashed line), 0.4 (dashed-dotted line), respectively.

ics simulations have been performed on three samples, made up by water solutions with HFIP molar fraction of 0.020, 0.082 and 0.400, respectively. These simulations allow for a direct comparison with the experimental results[239,240] and with the model developed by Fioroni *et al.*[216]

The interactions that take place in solution, varying the HFIP molar fraction, have been analyzed in terms of pair radial distribution function, taking in consideration a series of contacts to obtain insights on the formation of H-bonds and clusters. In particular, as previously suggested,[216] the pair radial distribution function related to the intermolecular interaction between central carbon atoms (C_c) (see Fig.4.6b) gives an estimate of the number of HFIP molecules that are involved in the formation of clusters. The coordination number at the distance of 9 Å reaches a value of 2.4, 4.7 and 6.4 for a HFIP molar fraction of 0.020, 0.082 and 0.400, respectively. The first two values are lower than those obtained by Fioroni *et al.*[216] and this behavior may be essentially related to the differences in the overall aspect of the pair radial distribution function, as a consequence of different potential adopted in the simulations.

The presence of a term to describe an interaction associated to the dihedral

angle $\phi_{\mathrm{H-C-O-H}}$ variation allows a more realistic description of the presence in the liquid of the two *ap* and *sc* conformation than the one proposed by Fioroni *et al.*[216] This behaviour extends also to the distribution function related to the H-bond interactions. By comparing the pair radial distribution functions, reported in Fig.4.7, related to the interaction with water, taking separately into account the $\mathrm{H}_{HFIP}\cdots\mathrm{O}_W$ (H-bond donor in Fig. 4.7a) and $\mathrm{O}_{HFIP}\cdots\mathrm{H}_W$ (H-bond acceptor in Fig. 4.7b) contacts with the results of Fioroni *et al.*,[216] similar results are obtained for the position of the most important features, whereas slight differences can be observed for the peaks height. In particular the coordination number for the H-bond donor interaction obtained by Fioroni *et al.*[216] ($\sim$2) is higher than that obtained in the present study, giving rise for this latter to a less structured liquid mixture.

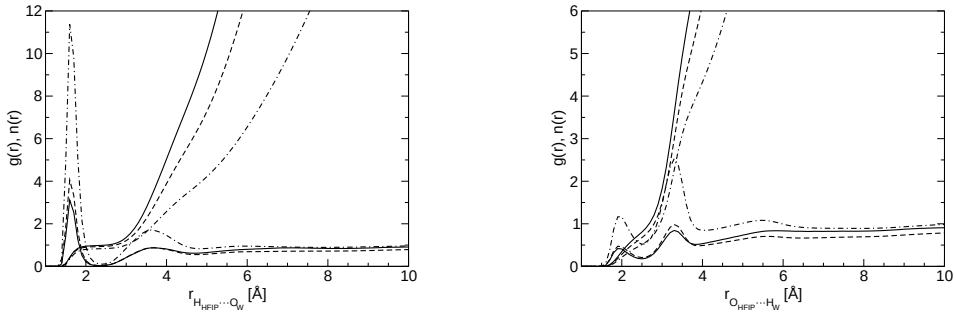

Figure 4.7: a) Pair radial distribution function for the donor $\mathrm{O}_w\cdots\mathrm{H}$ interaction at the molar fraction χ_{HFIP}=0.020 (black line), 0.082 (dashed line), 0.4 (dashed-point line), respectively; b)Pair radial distribution function for the acceptor $\mathrm{H}_w\cdots\mathrm{O}$ interaction at the molar fraction χ_{HFIP}=0.020 (black line), 0.082 (dashed line), 0.4 (dashed-point line), respectively

The differences in the H-bond interactions are still present also in the description of distribution functions related to the HFIP H-bond interactions, reported in Fig. 4.8. Also in this case the main features of the pair radial distribution functions compare with the results of Fioroni *et al.*,[216] with minor differences in the height of peaks.

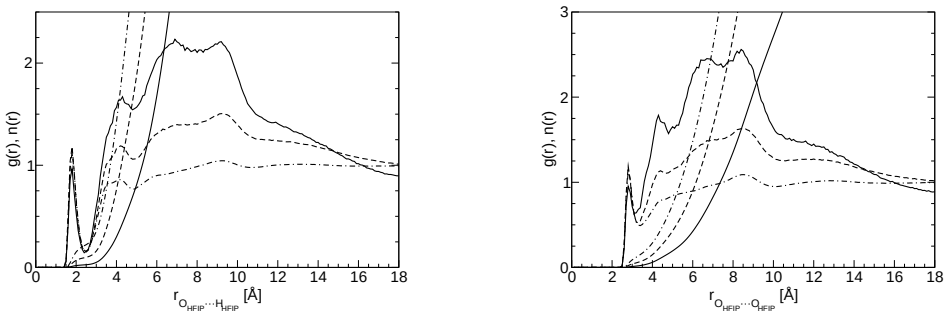

a) b)

Figure 4.8: Distribution functions for the solute-solute contacts. a) Pair radial distribution function for the O$\cdots$H interaction at the molar fraction χ_{HFIP}=0.020 (black line), 0.082 (dashed line), 0.4 (dashed-dotted line), respectively; b) Pair radial distribution function for the O$\cdots$O interaction at the molar fraction χ_{HFIP}=0.020 (black line), 0.082 (dashed line), 0.4 (dashed-dotted line), respectively.

A more detailed description of the structural organization of HFIP in water can be obtained from the analysis of the two-dimensional radial distribution functions reported in Fig. 4.9. In particular to state the interactions that take place at the three molar fractions χ_{HFIP}=0.020, 0.082, 0.400, the functions g(r_{OO},$r_{C_cC_c}$) related to the contacts O$\cdots$O and $C_c\cdots C_c$ (Figs. 4.9a, c, e) and g(r_{OO},r_{C_cO}) releated instead to the O$\cdots$O and $C_c\cdots$O contacts (Figs. 4.9b, d, f) have been plotted, respectively.

These analysis are a valuable help in the comprehension of the hydrophilic and hydrofobic interactions that HFIP molecules form in solution. In particular, as observed by X-ray,[222,240] X-ray small angle scattering[215,241] and IR experiments,[239] HFIP gives rise to micelle-like structures with a maximum at the molar fraction 0.082. In this respect it is important to verify the behavior in the three simulated samples. In fact, Fig. 4.9a, Fig. 4.9c and Fig. 4.9e show that, increasing the HFIP concentration, the organization of HFIP in solution undergoes strong structural changes. At low concentration (g(r_{OO},$r_{C_cC_c}$) of Fig. 4.9a) the interaction between HFIP molecules does not involve H-bonds, whereas they occur through the

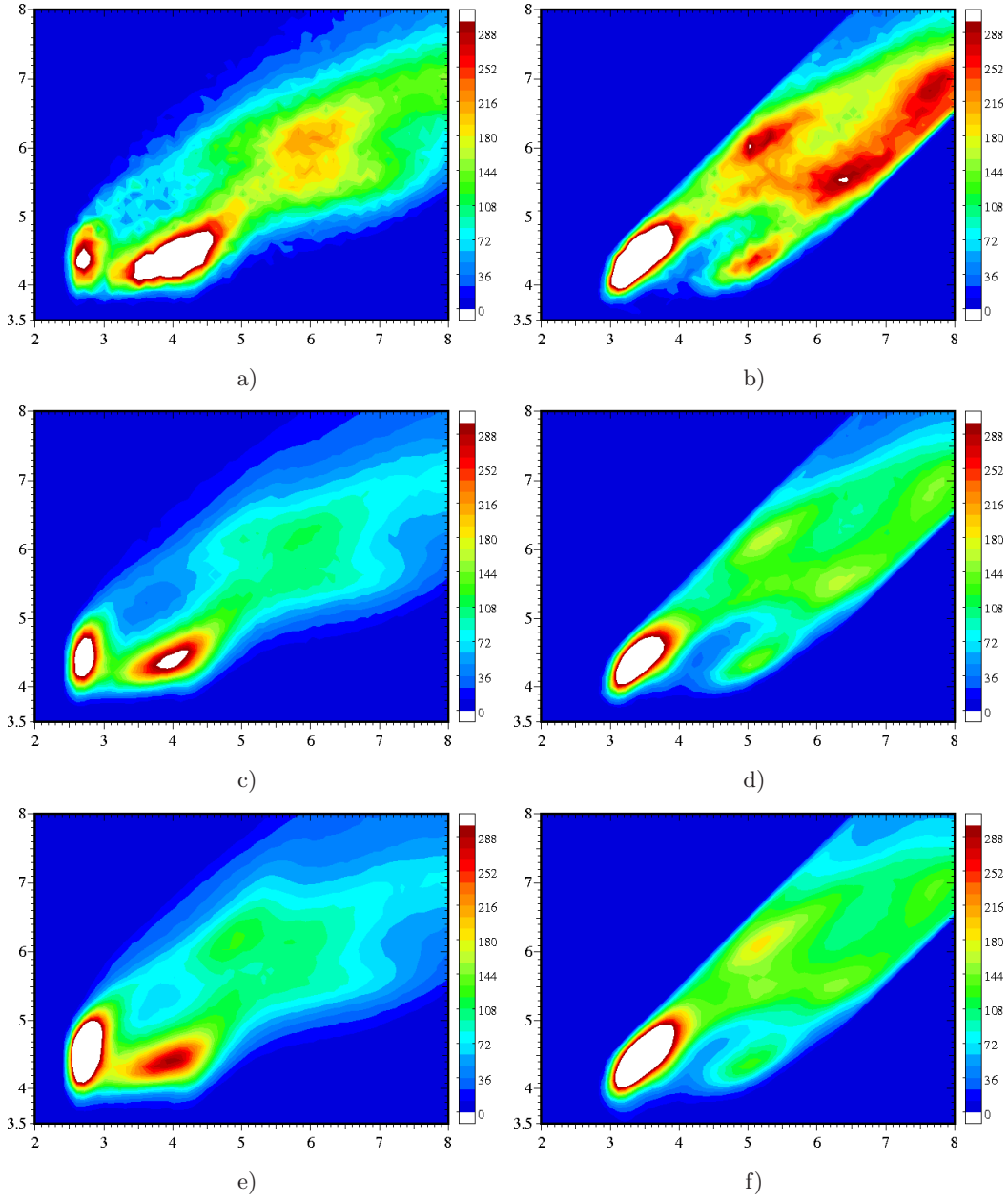

Figure 4.9: a) c) e) Two-dimensional radial distribution function $g(r_{OO},r_{C_cC_c})$. b) d) f) Two dimensional radial distribution function $g(r_{OO},r_{C_cO})$. The χ_{HFIP} molar fraction increases from top to bottom; a) and b) $\chi_{HFIP} = 0.020$; c) and d) $\chi_{HFIP} = 0.082$; e) and f) $\chi_{HFIP} = 0.400$.

hydrophobic part of the molecule. At this concentration HFIP forms H-bonds with water. With a HFIP molar fraction of 0.082 the alcohol molecules are involved both in hydrophilic and hydrophobic interactions and this behaviour can be a first explanation of the maximum of micelle-like clusters observed experimentally.[215,222,239–241] The surfaces show two maxima for the r_{OO} distances at about 2.8 and 4.0 Å and it confirms the dualism of HFIP in solution, namely the interaction with and without H-bond. For the more concentrated solution (lower panels), the H-bond interactions become the most inportant.

A similar description can be observed in the $g(r_{OO},r_{C_cO})$ two-dimensional distribution functions (Fig. 4.9b, Fig. 4.9d and Fig. 4.9f). In this case the growth of the H-bond interaction between the OH groups with increasing HFIP concentration is even more evident. In fact, by observing the surfaces for a r_{OO} distance of ∼2.8 Å, it is possible to note higher values for the maximum at the 0.400 molar fraction than at 0.020. On the contrary, the region related to the hydrophobic interaction becomes lower when increasing the HFIP concentration. It is important to note that during the simulations it has been observed, expecially at low concentration, that the formation of an improper H-bond of the hydrogen of the central carbon atom may occur. In this case the hydrogen atom bound to the central carbon atom is involved in a H-bond with the oxygen atom of a neighbour HFIP molecule. Similarly, short contacts with fluorine have been observed.

4.3 Hexafluoroacetone results

In order to understand the role in biochemistry of HFA as cosolvent in water solution and the interaction with proteins, a more detailed insight of the solvation mechanism has to be investigated along with the behaviour with respect to water molecules. HFA is made up by both hydrophobic and hydrophilic moieties[204,242] as depicted in Fig. 4.10a. The former, represented by the CF_3 groups, give rise to hydrophobic interactions with the alkylic side chains of polypeptides rather than the water molecules of the solution which are displaced far from the protein.[206,242] The

latter, represented by two OH groups, derive from the hydration of the molecule in water solution and let HFA belong to fluoroalcohol species. The hydrophobic parts of HFA are confirmed by the completely unstructured clustering of water molecules around the trifluoromethyl groups as shown in the pair distribution functions of Fig. 4.10b.

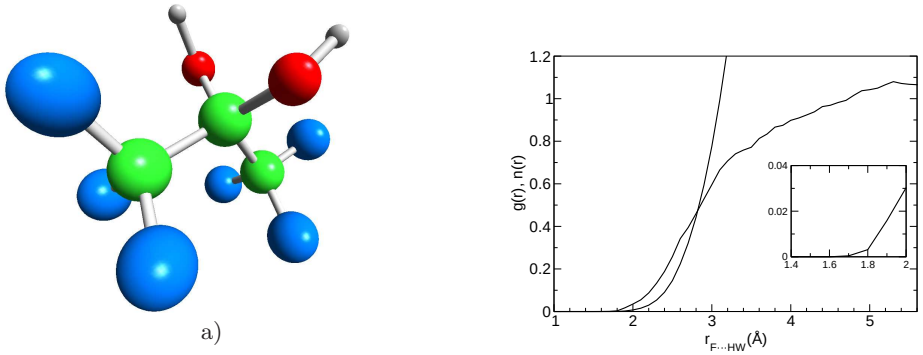

Figure 4.10: a) Representation of the structure of HFA. b) Radial distribution function and integration number between the fluorine and the hydrogen of water for HFA. The inset emphasizes the solvation distance of water molecules around the CF_3 groups (for more clarity the integration number is not shown).

This clearly shows the mobility of water molecules around the CF_3 groups and the lack of strong attractive interactions. The shortest distance between the hydrogen atoms of water molecules solvating the CF_3 groups and the fluorine atoms is about 1.6 Å as can be inferred from the inset of 4.10b.

This dehydrated environment around the protein favours the formation of a local hydrogen bond network between the peptides, with a strong stabilization of the α-helix structure. Moreover, the presence of hydrophilic OH groups on HFA gives rise to the formation of hydrogen bonds with the outer water molecules providing an increase of solubility.[242] Particular attention has been paid for the hydrogen bond structure through the study of the pair distribution function. The same criteria used in previous works for methanol and methanol solutions have been exploited to efficiently describe the H-bond structure.[34,48] The Fig. 4.11a shows that the OH

group is involved in H-bond with water through its hydrogen.

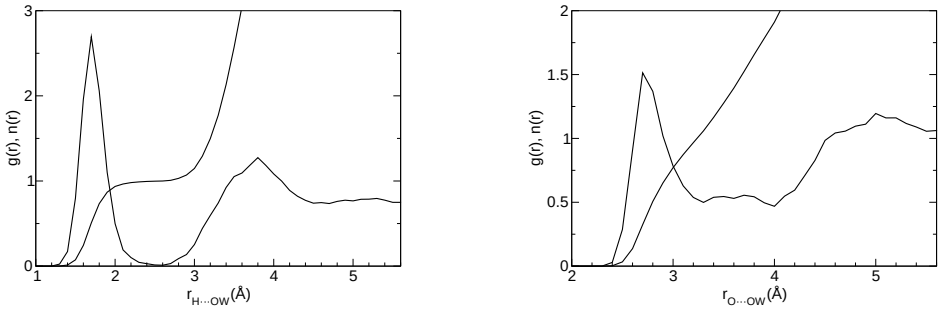

a) b)

Figure 4.11: a) Radial distribution function and integration number for the hydrogen of the OH group of HFA and the oxygen of water (labeled as OW). This trend describes the behaviour of the fluoroalcohol as H-bond donor; b) radial distribution function and integration number for the oxygen of the OH groups of HFA and the oxygen of water (labelled as OW).

The minimum at ∼2.5 Å is very deep and spread which is related to a difficult exchange between the H-bonded water molecule and the outer solvent molecules. HFA is H-bonded with water (the integration number at the minimum is of 1.0) and this interaction is quite stable. This is confirmed by the sharp maximum at ∼1.7 Å which denotes a small spread of the H$\cdots$O distance around this value.

The distribution function in Fig. 4.11b for O$\cdots$O between the oxygen atoms of HFA and water is slightly different. A minimum is present for HFA but it is not deep and flat. This can be attributed to large amplitude libration of the H-bonded water molecules.

The role of HFA as acceptor of H-bond with the oxygen of the OH groups is reported in Fig. 4.12a.

The maximum (around 1.9-2.0 Å) and the minimum (around 2.6 Å) are well defined showing the tendency to accept one H-bond upon the oxygen as can be inferred from the value of the integration number (∼1) at the first minimum of the g(r). The high hindrance that may occur for the couple of OH groups on HFA due

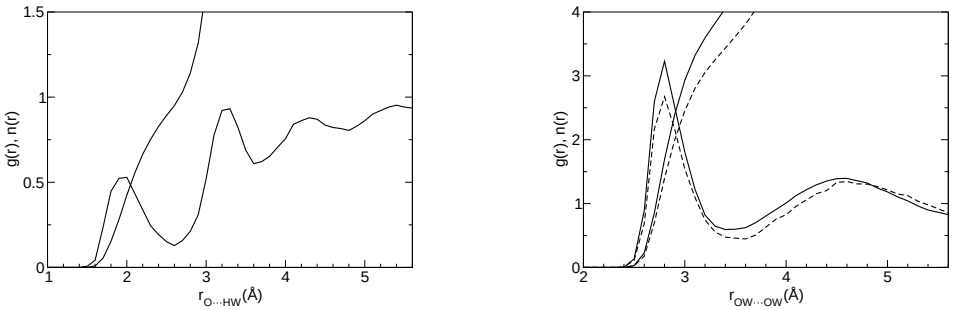

a) b)

Figure 4.12: a) Radial distribution function and integration number for the oxygen of the OH groups of HFA and the hydrogen of water (labelled as HW). This trend describes the behaviour of the fluoroalcohol as H-bond acceptor; b) radial distribution function and integration number of the oxygen-oxygen contact for the water molecules HFA. The contribution of water next to CF_3 groups is put in evidence (dashed lines) respect to the overall distribution (full lines). The cut-off distance (4.0 Å) for water molecules to define the CF_3 surround, has been retrieved from the radial distribution function of the C$\cdots$O contact (not reported).

to their dynamics in solution does not have any influence for the first shell of water molecules. Around 3.2 Å a narrow second peak can be noticed for HFA describing a second shell interaction. Again the presence of two indentical OH groups close to each other on HFA does not affect the capability to accept H-bonded solvent molecules. This trend can be immediately deduced from Tab. 4.2.

	hb_0	hb_1	hb_2
HFA1	26	70	4
HFA2	20	80	0

Table 4.2: Number of H-bonded water molecules accepted by HFA (hb_i). The data are reported in percentage (%) with respect the total time of the simulation. The contribution of each OH group on HFA (HFA1 and HFA2) has been reported.

The percentage of time without any H-bonded water molecules (hb_0 column in the Tab. 4.2) is 20 % for the less involved OH group of HFA. HFA accepts one

water molecule up to a value of 80 % of the simulation time (hb_1). The capability to accept more than one H-bonded water molecule (hb_2) is poor probably due to the presence of two OH groups that becomes significant for the hindrance between the solvent molecules.

The clustering of the water molecules in the bulk is not evidently affected by the presence of the fluoroalcohol, although a local disruption of the H-bond network for the solvent molecules around the trifluoromethyl groups occurs. In Fig. 4.12b the pair radial distribution function (along with the integration number) of the water molecules for the O$\cdots$O contact has been reported for the solution of HFA. The perturbation afforded by CF_3 groups is not significant for the peak and the minimum value that are in good agreement with respect to that of pure liquid at similar conditions both in theoretical[107,113,114,122,124,125,166,243–245] and experimental[246,247] investigations. The contribution of water molecules around the CF_3 groups has been separated in order to show the local perturbation on the solvent. At the minimum of the g(r), 3.4 Å, the integration number (3.4) is lower than the value expected for the usual tetra-coordination between water molecules in the pure liquid as reported in literature.[114,122,166,243,244] The tipical tetrahedral H-bond network[111] results to be locally perturbed only for the water molecules facing the trifluoromethyl groups and which are not able to form H-bonds with further solvent molecules. It implies a lower integration number at the minimum of the g(r) with respect to pure liquid at similar conditions.

The molecule of HFA is composed of two OH groups. The global statistics on both of OH groups has been taken into account for the plot of the distribution functions because of their very similar behaviour. This is put in evidence by Fig. 4.13 where the contribution of each OH group has been split in the distribution functions that better describe the solvation effects.

The contribution for both of the OH groups on HFA together with the characterization the H-bonds occurring between fluoroalcohol and solvent molecules is very similar. The main difference can be noted in the height of the first peak of the radial distribution functions of Fig. 4.13a, b, c due to a very slightly preferred interacton

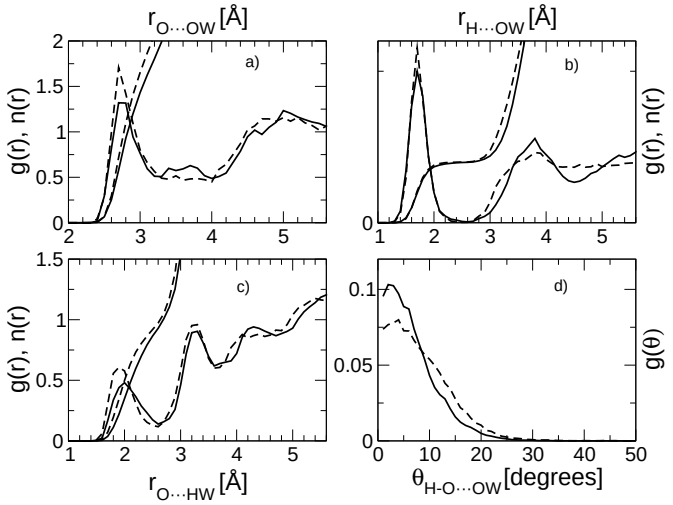

Figure 4.13: Radial and angular distribution functions The contribution of each OH group has been put in evidence with full or dashed lines. a) the oxygen-oxygen and b) the oxygen-hydrogen contact in the donation of H-bond; c) hydrogen-oxygen contact in the acception of H-bond with water; d) angular distribution function of the H−O· · ·OW contact.

for one of the OH groups. A little orientational distinction comes out also from the angular distribution function of Fig. 4.13d where a more narrow tail and a higher peak can be distinguished for one of the OH groups due to a distribution within shorter angle values.

A further characterization of the H-bond structure of HFA with water has been obtained by the g(r,θ) distribution functions using the same formalism as in previous works.[34,48]

The structural parameters for the donation of a hydrogen bond to solvent molecules are reported in Fig. 4.14a. A stable interaction can be argued either from the tight dispersion around the bond length at ∼1.7Å and from the directional character highlighted by the little tilt angle value (∼9°).

The contribution on the fluoroalcohol of H-bond as acceptor from the solvent molecules has also been investigated by the SDF depicted in Fig. 4.14b. The position

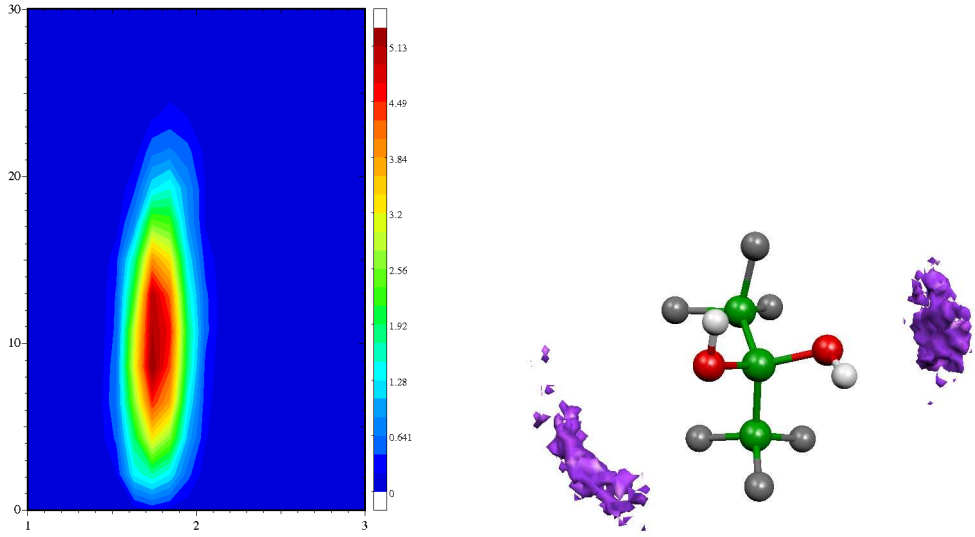

a) b)

Figure 4.14: a) Radial-angular distribution function of the H-bond of water for HFA as donor of H-bond. The cut-off parameters described in previous works are obtained from the analysis of the not normalized distribution functions for O$\cdots$H and H$-$O$\cdots$O contacts reported in Fig. 4.13b and Fig. 4.13d, respectively; b) SDF of the oxygen atom of water for HFA as acceptor of H-bond. The spots represent the positions spanned by the oxygen atoms of water H-bonded with the fluoroalcohol during the whole simulations.

spanned by the hydrogen atoms of water H-bonded around the oxygen atoms of the fluoroalcohol has been plotted showing dispersion due to the rotational degree of freedom of the OH groups for the dynamics in solution (see also Fig. 4.16 discussed later).

In order to perform realistic molecular dynamics simulations of biological systems in this cosolvent, a semi-empirical potential model is necessary. To check and modify available force fields, the Potential Energy Surface (PES) explored by HFA has been computed at a high level of theory for salient degrees of freedom, in particular for dihedral angles. This is shown in Fig. 4.15 where BLYP exhange-correlation functional (bottom panel) has been used in the density functional theory calculations for comparison with the *ab initio* simulations. HF calculations (top panel of Fig.

4.15) has been also reported to have agreement with the Amber procedure[248] in order to subsequently construct a reliable force field. The presence of the solvent molecules significantly affects the structure giving rise to different contour plots of the CPMD simulations with respect to isolated molecules. This is due to stable interactions of the OH groups with water molecules.

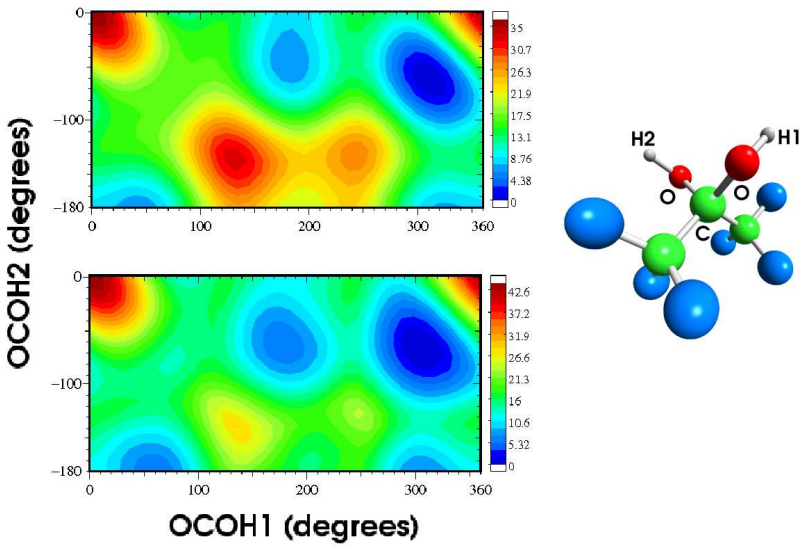

Figure 4.15: PES of HFA as a function of OCOH1 versus OCOH2 dihedral angles. The calculation has been performed at HF/6-31g(d,p) (top panel) and BLYP/6-31g(d,p) (bottom panel) level of theory. Energy data in the right panel are expressed in kJ mol^{-1}. The picture aside shows a HFA configuration. The label on the atoms define the dihedral angles to be considered.

Low energy configurations are arranged around 300° and -60° for OCOH1 and OCOH2, respectively, and can be found with high probability even in water solution (as shown in Fig. 4.16). A further minimum is noticed around 180° for OCOH1 and -40° for OCOH2 not explored during the CPMD simulation in water solution. In the isolated molecule the OH groups point directly towards the F atoms of CF_3 to stabilize the structure through H$\cdots$F intramolecular interactions. In solution, because of the affinity of the OH groups for water, the interaction with the solvent molecules is preferred. The dynamics in water solution gives rise to a higher spread

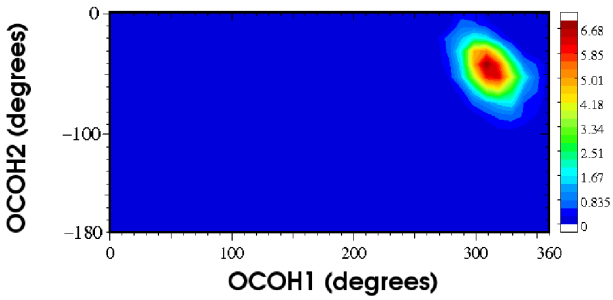

Figure 4.16: OCOH1 versus OCOH2 dihedral angles distribution for HFA obtained from the CPMD simulation.

of the dihedrals to lower angular values. The "all electrons" calculations in Fig. 4.15 also show that the two maxima around (0°,0°) and (360°,0°) (in OCOH1,OCOH2 coordinates) are located at high energy with respect to the minimum (∼30 kJ mol^{-1}, much higher with respect to ∼2.49 kJ mol^{-1}, that is the value of kT at 300 K) and they are not overcome in the water solution dynamics at finite temperature in which such configurations are not explored (see Fig. 4.16).

The different configurations generated by the degrees of freedom of the dihedral angles in vacuum may be responsible of heavy variations in the dipole moments and this may affect the behaviour in solution, as it has been reported in literature for HFIP.[223]

Studies on polarization effects have been performed for HFA with explicit solvent molecules and with the Polarizable Continuum Model (PCM)[249–252] in order to have a more detailed understanding on the contribution of the solvent in polarization effects. "All electrons" calculations in vacuum reported in Tab. 4.3 emphasize the contribution brought by the water molecules in enhancing the polarization of HFA in solution.

In Tab. 4.3 the dipole moment values from "All electrons" calculations on the fluoroalcohol are shown either for isolated molecules, or explicitly adding H-bonded water molecules, or in presence of a PCM water solvent. The contribution of the H-bonded water molecules significantly affects the dipole moment. The ratio of

	Dipole moment (D)
$< \mu >_{solvent}$	2.9 ± 0.3
$< \mu >_{solute}$	4.7 ± 0.8
$\mu_{isolated}$	2.2
+ 1 H_2O	4.4
+ 2 H_2O	4.9
PCM (non opt)	3.0
PCM (opt)	4.3

Table 4.3: Average dipole moment values (in Debye, D) and relative standard deviation for HFA ($< \mu >_{solute}$) and for the water molecules ($< \mu >_{solvent}$) deriving from CPMD simulations. Data from "all electrons" calculations are also reported for the isolated molecule at the BLYP/6-311++g(3df,3pd) ($\mu_{isolated}$) level of theory. One or two water molecules have been explicitly added to the isolated solute molecule (+ 1 H_2O, + 2 H_2O). PCM calculations have been performed without optimization of the solute structure (PCM non opt) and after optimizing the solute geometry (PCM opt) in order to have the effect of the structural rearrangement on the dipole moment. All standard settings have been adopted for PCM model.

the dipole moment by adding one water molecule with respect to the value of the HFA isolated molecule ($\mu_{isolated}$) is double (with an increment going from 2.2 D to 4.4 D). This ratio is more than double when adding two water molecules (increasing from 2.2 D to 4.9 D). In the PCM model the increase of the dipole moment, after the geometric optimization of the solute molecule, correctly describes the structural rearrangement due to the dielectric environment. The addiction of water to the isolated solute molecule well reproduces the dipole moment of the PCM model with the optimized solute structure. Going from the isolated molecule of HFA to the non-optimized structure in PCM, an increment of the dipole moment from 2.2 D to 3.0 D occurs. No evident variation is noticed going from the solute molecule with one H_2O to the isolated molecule optimized in PCM (from 4.4 D to 4.3 D). The contribution of the dielectric is almost totally satisfied by the presence of the first H-bonded water molecule pointing out the stability of the solvent molecules interacting with the fluoroalcohol. The average dipole moments from the CPMD simulation are also

reported in Tab. 4.3. The presence of the fluoroalcohol does not significantly affect the average dipole moment of the solvent ($< \mu >_{solvent}$ = 2.9 D) which is not far from the value of the pure liquid in similar conditions (about 3.0 D),[113,114] whereas an average higher value is observed for HFA ($< \mu >_{solute}$ = 4.7 D).

A different polarization has been observed from CPMD simulations for water molecules directly connected to the fluoroalcohol whether it is donor or acceptor of H-bonds. The polarization effects of HFA on the solvent is shown in Fig. 4.17 where the contribution of the water molecules H-bonded to the fluoroalcohol is put in evidence.

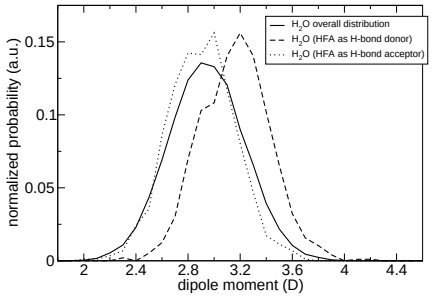

Figure 4.17: Dipole moment distribution for water molecules in HFA (solid line) obtained from the calculation of the WFCs. The contribution of water H-bonded to HFA as a donor and as an acceptor of H-bond is also reported in dashed line and dotted line, respectively.

A higher polarization is noticed for the water molecules bonded via the oxygen atom ($\Delta\mu \sim$ +0.15 D), whereas slightly lower values of the dipole moment ($\Delta\mu \sim$ -0.03 D) can be reported for the water molecules H-bonded to the fluoroalcohol through the hydrogen atom. The water molecules undergo a different polarization effect whether they donate hydrogen atom to the solute molecule or accept H-bond from the hydrogen of HFA. This is probably due to the orientation of the dipole moment vector of the water molecules H-bonded with the oxygen atom that is very similar to the H-bond direction.

4.4 A case study: melittin in hexafluoroisopropanol/water solution

The study on HFIP and HFA interaction with water solutions represents the starting point to evaluate the stabilization effects of these fluoroalcohols with respect to proteins or short polypeptide chains. Since α-helix stabilization has been noticed in HFIP/H_2O mixtures at 30% (v/v) in HFIP,[209,253] a classical MD has been performed on MLT in HFIP/water mixture ($\chi_{\mathrm{HFIP}} = 0.082$) by adopting the new semi-empirical potential derived from the *ab initio* computations.

MLT is a residue of 26 AminoAcids (AAs) of the *Apis Mellifera* venom[254] and it has been noted to assume an unfolded structure with the absence of fluoroalcohols.[222] The presence of HFIP as fluorinated cosolvent in water solution allows the stabilization of the secondary structure of the polypeptide which more steadily goes toward an α-helix conformation.

The structural parameters for the HFIP-HFIP and HFIP-H_2O interactions are successfully described and reported in Fig. 4.18 where the distribution functions of cosolvent-cosolvent and cosolvent-solvent are in good agreement with that found in the previous HFIP/water mixtures with $\chi_{\mathrm{HFIP}} = 0.082$.

The perturbation afforded by MLT is negligible on the average of the solution. To evaluate the contribution due to the presence of the MLT a distribution function of the molar fraction of HFIP has been reported for every AA of the polypeptide as depicted in Fig. 4.19.

A two-dimensional plot comes out from the analysis enlightening a higher concentration of HFIP near the side chains of the AAs around 6 Å away from the backbone of the peptide. In the middle of the chain, there is a lack of HFIP concentration around the AA numbered 10 and 11 that are two THR residues. In this position a local disruption of the α-helix occurs on MLT with the formation of two bent helix regions.[209,217] After $\sim$20 ns of the simulation a partial loss of α-helical structure is noted as can be seen from Fig. 4.20.

A higher concentration of HFIP molecules are also noticed near MLT with the

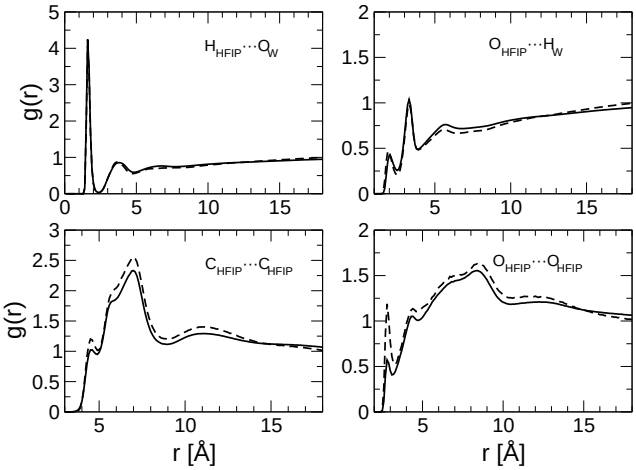

Figure 4.18: Pair radial distribution functions for HFIP-H_2O (top panels) and HFIP-HFIP (lower panels) interactions for the MLT simulation (full lines). Dashed lines refer to the corresponding distributions of HFIP/water mixture ($\chi_{\mathrm{HFIP}} = 0.082$).

formation of a hydrophobic environment around the protein. The affinity between the hydrophobic side chains of the peptide and the fluoroalcohols molecules keep HFIP close to MLT. The water molecules are hindered and they are not able to interact with the side chains in order to disrupt the H-bond between the AAs. After 20 ns of simulation in water the protein completely loses the secondary structure,[217] whereas α-helix organization is still present in HFIP/water mixture with $\chi_{\mathrm{HFIP}} = 0.082$.

4.5 Conclusions

CPMD simulations have been performed on HFIP and HFA to characterize the interactions of fluoroalcohols in water solution. A new force field has been constructed for HFIP and the results of classical MD simulations have been compared to the *ab initio* calculations with a good agreement. The force field has been adopted to describe HFIP/water mixtures through classical MD simulations and cluster forma-

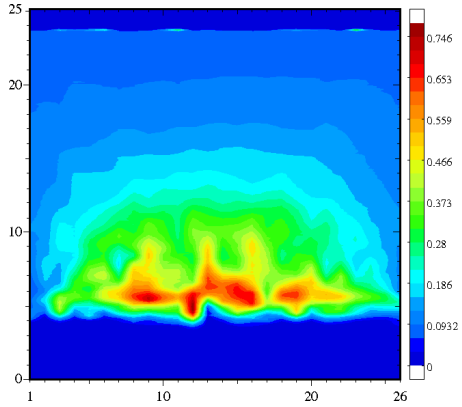

Figure 4.19: Two-dimensional distribution function of the molar fraction of HFIP around every AA. The aminoacidic residues are GLY-ILE-GLY-ALA-VAL-LEU-LYS-VAL-LEU-THR-THR-GLY-LEU-PRO-ALA-LEU-ILE-SER-TRP-ILE-LYS-ARG-LYS-ARG-GLN-GLN from left to right and they are numbered from 1 to 26 on x-axis.

tion of solute and solvent molecules has been noticed. The stabilization effects on the secondary structure of short polypeptides are well known for water solutions of fluoroalcohols and an accurate force field is necessary to correctly describe the occurring interactions. A classical MD simulation has been consequently performed on MLT with HFIP/water mixture showing the strong stabilization of the α-helix conformation of the peptide.

The new classical force field correctly describes the interactions between HFIP and water and a good agreement of the solvation shell of the fluoroalcohol is noticed in comparison to the results obtained by the *ab initio* simulations. An evident micelle-like structure of the solution can be deduced from the classical simulations of HFIP/water mixtures. A higher cluster organization with the most used HFIP molar fraction of $\chi_{\mathrm{HFIP}} = 0.082$ is noticed due to hydrophobic and hydrophilic interactions. The interacton of the ordinary HFIP/water mixture with short polypeptides has been satisfactory reproduced by a classical MD simulation on MLT. The stabilization of the secondary structure of MLT has been shown due to coating effects of HFIP around the protein. A high concentration of HFIP has been noticed around the

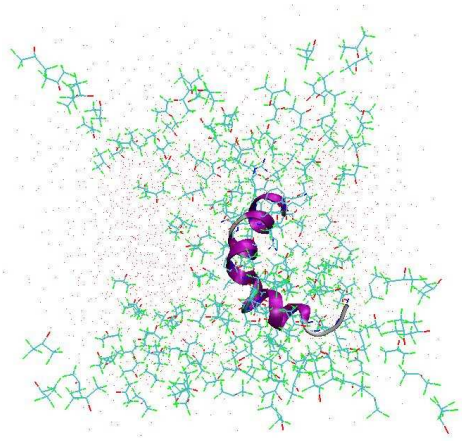

Figure 4.20: Snapshot extracted from the sumulation after 20 ns that shows that the α–helix is bent on the position of THR-THR in the middle of the chain. Hydrogen atoms are omitted for clarity of the representation.

peptide chain forming a hydrophobic environment with the almost total absence of water molecules directly interacting with the MLT. The α-helix conformation has been observed during the whole simulation run. A local and slight disruption of the helix occurs in the middle of the chain at the position of two adjacent threonine residues.

5

Open-addiction versus cyclo-condensation of organic compounds

The reaction of primary nitro compounds with electron-deficient olefins under base catalysis[255,256] gives two different products as reported in Fig. 5.1 and by Trogu *et al.*[257] When the dipolarophile is electron-poor and it is mainly made up by a molecule with double bond conjugated with an electron withdrawing group (EWG) and it is indicated as Michael acceptor, a competition is observed between cycloaddiction-condensation (*i*) and conjugate addiction (*ii*).

The conjugate addiction of a nitro compound to an electron-deficient olefin may follow a Michael-type reaction giving open-chain adducts (*i*). A cycloaddiction-condensation path may be also attempted yielding isoxazole derivatives from the cycloaddiction of nitrile oxide to double bonds with water elimination (*ii*). The results strongly depend on the dipolarophile, namely the electron-deficient olefin, and on the reaction conditions, mainly the temperature.[257] The activation of nitro compounds under base catalysis is better achieved with two-basic centers bases such as 1,4-diazabicyclo[2.2.2]octane (DABCO) for its H-bonding capabilities[257] and the formation of the H-bonded salt is observed. The optimized geometry of the complex nitroacetate-DABCO is depicted in Fig. 5.2 where two possible structures have been taken into account.

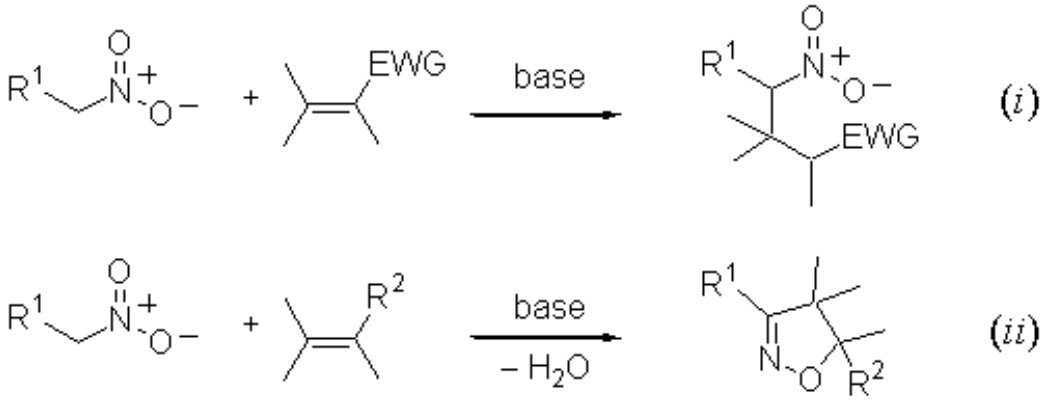

Figure 5.1: Base catalyzed reaction paths of nitro compounds with electron-deficient olefins. R_1 is a generic functional group and EWG represents generic electron withdrawing groups. R_2 may be an EWG such as CN, CO_2Me, COMe, $CONMe_2$ or SO_2Ph.

The complex depicted in Fig. 5.2b, where the hydrogen is shared by two oxygen atoms of the nitro compound, is slightly lower in energy by 0.77 kJ mol^{-1} than the one in Fig. 5.2a, where a single O$\cdots$H interaction occurs. In Fig. 5.2b the hydrogen is optimized at $\sim$ 1.66 Å and $\sim$ 2.06 Å far from the NO_2 and the C=O, respectively. A shorter distance ($\sim$ 1.35 Å) is reported for the single O$\cdots$H interaction of the structure in Fig. 5.2a with respect to that found for the other complex, whereas the acid hydrogen is drawn further from DABCO ($r_{NH} \sim 1.17$ Å) than the distance reported for the complex of Fig. 5.2b ($r_{NH} \sim 1.07$ Å).

The addiction of a copper salt in the solution drifts almost quantitatively the reaction path in *ii* obtaining the cycloadduct as the only reaction product. A catalytic effect of Cu^{2+} on the condensation of primary nitro compounds with dipolarophiles has been evidenced.[257] In order to rationalize the role of Cu^{2+} ion in favouring the cycloadduct formation with respect to the open-chain adduct through the Michael reaction, some *ab initio* calculations have been performed on the species present in solution. Nitroacetic methylester, DABCO and acrylonitrile have been selected to perform the search of the structural minima in vacuum with a series of geometrical optimizations. The *ab initio* "all electrons" computations have been executed by

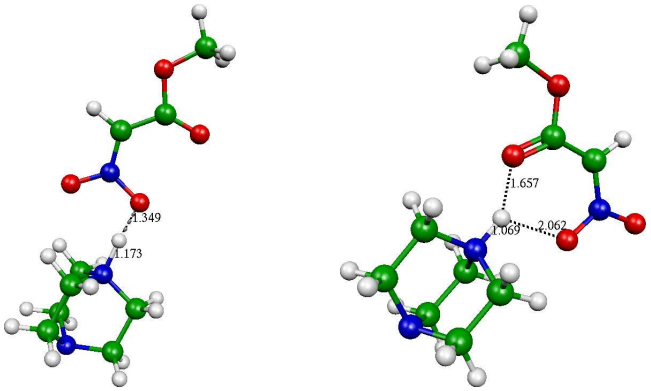

a) b)

Figure 5.2: Two possible interactions of DABCO with nitro acetic methylester to activate the nitro compound; a) the hydrogen interacts with only the NO_2 of the nitro ester; b) the hydrogen is shared between the oxygen of the NO_2 and the C=O groups. The structures have been optimized at B3LYP/6-31d(d) level of theory.[258]

Gaussian[259] and Gamess[260,261] programs. The reagents have been chosen to reduce the computational load and contemporaneously assure the correct behaviour in the two reaction paths at 30°C or 60°C.[257]

Single reagents, products and intermediates, have been initially optimized with Gamess at B3LYP/6-31g(d) level of theory[258] and the corresponding energies are summarized in Tab. 5.1.

The species involved in the reaction paths are reported in Fig. 5.3 where the overall mechanism of electron transfer is represented by arrows.

Nitroacetic methylester undergoes a tautomerization mechanism in which an acid hydrogen is delocalized in the molecule between the NO_2- and the $MeCO_2-$ groups. The energy obtained from the *ab initio* calculations of the species **1a** and **1b** involved in the equilibrium show a lower value for **1a** of 17.83 kJ mol^{-1} with respect to **1b**. The high barrier of the transition state **1ab** (not reported in Fig. 5.3) has to be overcome in vacuum (251.07 kJ mol^{-1} with respect to the energy of **1a**) to reach the equilibrium from **1a** to **1b** and *viceversa*. The stabilization due to the solvent and the temperature of the reaction environment allow the presence of both

	E
1a	-472.6427626572
1b	-472.6359719892
1ab	-472.5471360426
2a	-170.7284015125
3a$^-$	-642.8416693171
3a	-643.4081098199
4a	-567.0417675714
DABCO	-345.1018134623
DABCO-H$^+$	-345.4864851210

Table 5.1: Energies in atomic units (Hartree) obtained from *ab initio* calculations at B3LYP/6-31g(d) level of theory for some species involved in the reaction mechanism. The labels refer to the species depicted in Fig. 5.3.

the tautomers in solution. At this point DABCO acts on the acid hydrogen of **1b** in order to activate it as methyl nitro acetate. The complex obtained represents the reactant on which either cycloaddiction (*path A*) and/or Michael conjugate addiction (*path B*) may occur when reacting with acrylonitrile **2a**.

The final step of the Michael open-chain addiction is represented by the proton transfer from DABCO-H$^+$ to **3a**$^-$ as it can be seen from the reaction scheme of Fig. 5.3. Energy structure optimization has been performed by "all electrons" *ab initio* calculations on the intermediate **3a**$^-$ and the protonated DABCO (labelled DABCO-H$^+$) and their energy has been reported in Tab. 5.1 together with the corresponding neutral species. The energy of the anionic species **3a**$^-$ is 1487.19 kJ mol^{-1} with respect to **3a**, whereas the energy of DABCO-H$^+$ is -1009.96 kJ mol^{-1} with respect to DABCO. The proton transfer from DABCO-H$^+$ to **3a**$^-$ is then favoured and the energy balance justifies the completion of the Michael reaction at work temperature of 30° or 60°.[257]

In order to explain the effects due to the presence of Cu^{2+}, a series of calculations has been performed to obtain reliable copper complexes, considered the sensible species responsible of the quantitative preference for the cycloaddiction path with

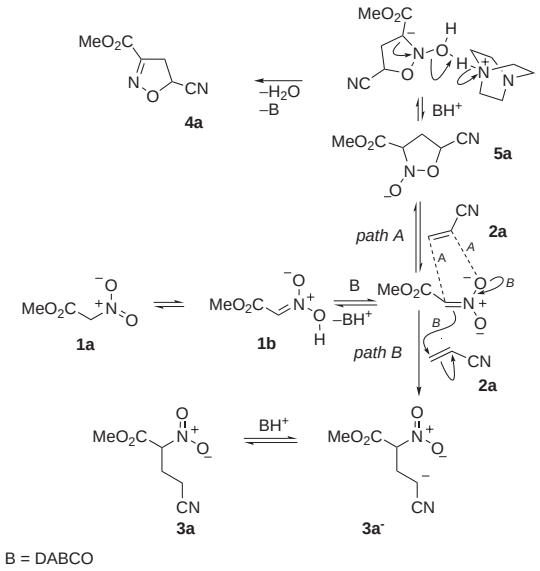

Figure 5.3: Overall reaction mechanism. Reagents are different from that reported by Trogu *et al.*[257] according to the species taken into account for the calculations.

these reagents.

Nitroacetic acid dianion has been reported to give strong complex with Cu^{2+}ion[262] and by analogy a similar behaviour with the monoanion of nitroacetic ester may be described.[263] Possible Cu^{2+}-complexes have been hypothesized to explain the role of Cu^{2+} to drive the reaction toward the cycloadduct. A reasonable complex of Cu^{2+} is coordinated by nitroacetate through the oxygen of the acetic group and the oxygen of the nitro group[262,263] in equatorial position to form a squared base of an octahedral coordination for this ion in solution. The axial positions are occupied by DABCO which is present in solution with the formation of Cu−N interactions. NMR spectra in absence of nitrocompounds show a good coordination of Cu^{2+} with DABCO. Since Cu^{2+} is a paramagnetic metal ion, it affects NMR spectra by leading to broad or undetectable signals and a relaxation rate increase is observed.[264] By this way, when a catalytic quantity of Cu^{2+} is added, the signals of DABCO disappear in the NMR spectra and the formation of Cu−N interactions occurs. Two configurations have been obtained and they are reported in Fig. 5.4.

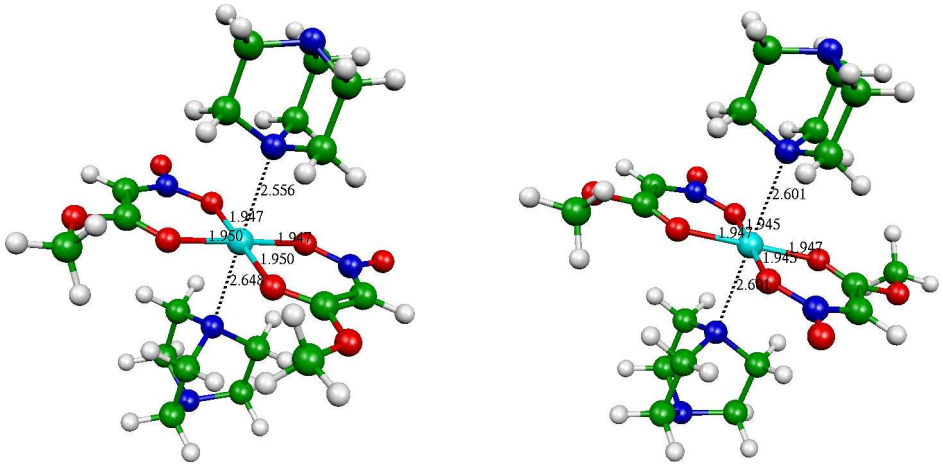

a) b)

Figure 5.4: Cu complexes; a) a symmetry plane is present giving rise to a C_s group of symmetry; b) an inversion center is present implying a C_i symmetry group of the complex.

The 6-31g(d) basis set has been chosen both for Cu^{2+} and for the organic species even if a lanl2dz basis type may be more appreciable in describing the metal ion. More accurate calculations may have little influence on geometrical structure of the whole complexes, but they can be subsequently performed to obtain refined structural data such as distances or angles. Starting from complexes without symmetry, the geometry optimization have led to structures belonging to the C_i and the C_s point group. The C_i complex of Fig. 5.4b is lower in energy by 4.36 kJ mol^{-1}. The small difference in energy states that both complexes may exist in solution at work temperature with a little preference for the C_i configuration with respect to the C_s of Fig. 5.4a. The stabilization is probably due to the methyl groups which are far from each other because no other change occurs between the structures.

Since at work temperature both Cu-complexes may be present in solution, acrylonitrile has been subsequently added to the C_s and the C_i complexes and further geometric optimizations have been performed. The dipolarophile has been put initially in the most favourable position to interact with the methyl nitroacetate to give rise to the cycloaddiction. The final corresponding structures are represented

in Fig. 5.5.

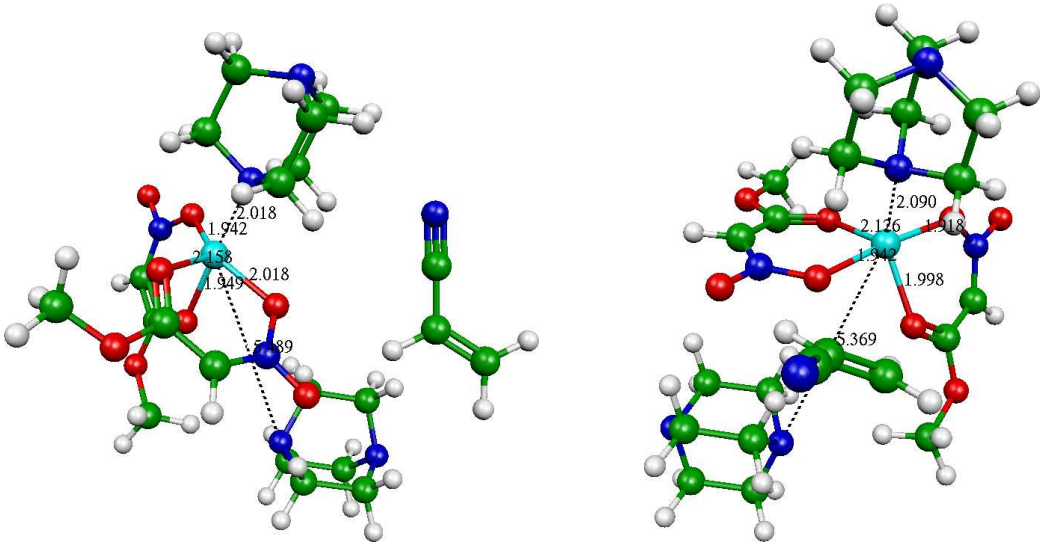

a) b)

Figure 5.5: Optimized geometry for the complex of Cu with two molecules of methyl nitroacetate and two molecules of DABCO after the addiction of acrylonitrile near a nitroacetate; a) structure coming from the C_s complex of Fig. 5.4a; b) structure deriving from the C_i complex of Fig. 5.4b.

For both complexes, during the optimization steps, one DABCO gets far away from the coordination of Cu^{2+}, whereas a distorted structure is assumed by the complex leaving the octahedral configuration. The acrylonitrile gets off the position near the nitroacetate and rearrange in a way that the atoms do not interact anymore each other to encourage the cycloaddiction. The difference in energy between the configurations is 22.74 kJ mol^{-1} where the lower in energy now is the structure of Fig. 5.5a coming from the C_s complex of Fig. 5.4a. A greater stabilization is therefore noticed in the optmization of the C_s complex after the addiction of acrylonitrile with respect that observed for the C_i complex.

For clarity in the interpretation, the salient structural data derived from the C_i and the C_s complexes are also reported in Tab. 5.2 where the changes in the coordination distances of Cu^{2+} are highlighted.

complex type	contact	before	after
	Cu−O_1 (NO_2)	1.945	1.918
	Cu−O_1 (CO)	1.947	1.998
C_i	Cu−O_2 (NO_2)	1.945	1.942
	Cu−O_2 (CO)	1.947	2.126
	Cu−N_1	2.601	2.090
	Cu−N_2	2.601	5.369
	Cu−O_1 (NO_2)	1.947	2.018
	Cu−O_1 (CO)	1.950	2.518
C_s	Cu−O_2 (NO_2)	1.947	1.942
	Cu−O_2 (CO)	1.950	1.949
	Cu−N_1	2.648	2.018
	Cu−N_2	2.556	5.489

Table 5.2: Changes of Cu^{2+} coordinative distances (in Å) for the C_i and the C_s complexes before and after the addiction of the dipolarophile.

The addiction of the dipolarophile gives rise to a global reorganization in the structures of the complexes leaving the octahedral coordination in favour of a more distorted square based pyramid. In both complexes the neat increase of a Cu^{2+}-DABCO distance (Cu−N_2) from 2.601 Å to 5.369 Å for C_i and from 2.556 Å to 5.489 Å for C_s denotes the loss of the coordinative site by one DABCO. The distance of the other base (Cu−N_1) shortens by more than 0.5 Å in both cases (from 2.601 Å to 2.090 Å for C_i and from 2.648 Å to 2.018 Å for C_s) giving rise to a stronger interaction between the species. The initial symmetry of the complexes (C_i and C_s point groups) is lost when adding acrylonitrile. For the oxygen atoms in the equatorial position, the distances Cu−O_1 and Cu−O_2 between similar functional groups of nitroacetate (NO_2 and C=O) with Cu^{2+} break the symmetric distribution.

The B3LYP/6-31g(d) calculations have been performed for the structure of the Cu^{2+} complexes. This level of theory does not reproduce van der Waals effects and they may be representative of the stabilization of acrylonitrile in such a position to favour the cycloaddiction. The search of a minimum as a good starting point to have

the cycloaddiction may be successfully achieved when considering van der Waals long range forces. This can be obtained by more accurate calculations at MP2 level of theory[265] even if a larger computational load and resource have to be considered together with a longer execution time concerning this kind of calculations.

6

Conclusions

Car-Parrinello Molecular Dynamics (CPMD) has been employed as a very robust and predictive tool to study molecular systems in condensed phase. Starting from the work by Car and Parrinello,[11] *ab initio* Molecular Dynamics (MD) has been applied in many different fields, from semiconductor solid-sate physics to liquids and solutions,[14] giving rise to new approaches for the scientific research. Despite of the heavy computational load due to the *a priori* determination of an *ab initio* potential[32] by a variational principle, CPMD is one of the most appreciated scientific technique in order to predict salient molecular properties on systems ranging from simple models to large scale biological systems.[33] The success of this method has also grown during the years with the development of more and more powerful parallel supercomputers. Steps forward have been made in technological fields providing the thrust to investigate more complex systems.

The arguments highlighted in the previous chapters have mainly dealt with the microsolvation of the neighbour molecules forming the coordination shell in protic solutions. The effects on the solvation may affect many general properties of the solutions and then may influence their employment in chemistry matters. In particular solvation dynamics of simple ionic species, alkaline and alkaline-earth ions

or anions such as bromide, has been studied in liquid methanol. These systems are important to obtain an exhaustive picture of the interactions occurring in protic self-associating solvents with charged species. Solvation shells are involved in changing the effective ionic radii and they affect the transport of the ions through biological ion channels. Colligative properties and diffusion in solution are also connected to the interaction of ions with solvent molecules together with the formation of solvent shells.

Fluorinated cosolvents in aqueous solution has been initially investigated by *ab initio* MD in order to build accurate force fields for subsequent classical MD simulations. Biochemical relevance concerns fluorinated alcohols such as 1,1,1,3,3,3-hexafluoroisopropanol (HFIP) and 1,1,1,3,3,3-hexafluoroacetone, because of their use as cosolvents in water solution to stabilize the secondary structure of short polypeptide chains. Classical MD simulations have been performed on HFIP/water mixtures as a starting point to understand the effects of these solutions in a proteic context. The stabilization effects on the secondary structure of short polypeptides have been successfully evidenced by the classical MD simulation on Melittin in the ordinary HFIP/water mixture (HFIP molar fraction $\chi_{\mathrm{HFIP}} = 0.082$).

CPMD gives an exhaustive description of the structural properties of many molecular systems in condensed phase taking into particular account charge effects and electronic rearrangement. Very sensitive properties such as electronic distribution or charge transfer may give a decisive influence on the macroscopic behaviour of a solution. Investigations on the structure of the solvation shell have been obtained by the analysis of the distribution functions, whereas electronic properties have been treated in terms of dipole moments, with the maximally-localized Wannier functions, and charge transfer, with the Atoms In Molecules (AIM) population analysis. These methods allowed to confirm the stabilization of the solvation shells by means of electrostatic contributions and they put in evidence the strong polarization on the first solvation shell molecules due to the presence of charged species. By this way, electronic distribution studies are very important to understand the effects of charge transfer in polarizable systems. The computational time of the analysis

to obtain significant results is often comparable to the whole simulation time itself and this is mainly due to the large amount of data to be processed. In order to obtain results over a great number of configurations extracted from a trajectory, the parallelization of a code for the AIM charge analysis, with the method proposed by Bader, has been implemented. The very portable strategy adopted allow to apply the scheme to a large variety of systems where the necessity to simultaneously compute indipendent configuration files occurs. A great improvement has been noticed by adopting a *Master-Slave* method for the parallelization of the code and the computational resources hosted at CINECA showed an execution time up to ~ 100 times faster than the serial algorithm.

Orgnanic compounds, such as nitro esters activated by base catalyst, react with electron deficient olefin in order to give two possible reaction paths. The formation of isoxazole derivative cycloadducts are quantitively observed when introducing copper(II) salts in solution with a cycloaddiction/condensation mechanism. The cyclodduct competes with the formation of an open-chain product coming from a simple Micheal addiction in absence of Cu^{2+}. *Ab initio* calculations have been performed in order to comprehend the role of Cu^{2+} in the reaction mechanism. Optimized geometries of possible Cu^{2+}-complexes in work solution have been obtained by "all electrons" calculations using gaussian basis sets. It has been shown that the consideration of van der Waals long range forces is important to accurately describe the cycloaddiction mechanism due to the presence of Cu^{2+}. The good positioning of the reactive species to favour the cycloaddiction is a very sensitive parameter and Van Der Waals interactions may lead to correctly reproduce the reaction mechanism.

Bibliography

(1) Hohenberg, P.; Kohn, W. *Phys. Rev.* **1964**, *136*, B864–B871.

(2) Kohn, W.; Sham, L. J. *Phys. Rev.* **1965**, *140*, A1133–A1138.

(3) Schröedinger, E. *Ann. Phys.* **1926**, *79*, 361–376.

(4) Schröedinger, E. *Ann. Phys.* **1926**, *80*, 489–527.

(5) Thomas, L. H. *Proc. Cambridge Philos. Soc.* **1927**, *23*, 542–548.

(6) Fermi, E. *Rend. Accad. Naz. Lincei* **1927**, *6*, 602–607.

(7) Kohn, W. *Rev. Mod. Phys.* **1999**, *71*, 1253–1265.

(8) Meot-Ner, M. *Chem. Rev.* **2005**, *105*, 213–284.

(9) CPMD consortium page, http://www.cpmd.org/.

(10) *CPMD V 3.9 Copyright IBM Corp 1990-2004*; Copyright MPI für Festkörperforschung: Stuttgart, 1997-2001.

(11) Car, R.; Parrinello, M. *Phys. Rev. Lett.* **1985**, *55*, 2471–2474.

(12) Tse, J. S. *Ann. Rev. Phys. Chem.* **2002**, *53*, 249–290.

(13) Hutter, J.; Iannuzzi, M. *Z. Kristallogr.* **2005**, *220*, 549–551.

(14) Hutter, J.; Curioni, A. *Chem. Phys. Chem.* **2005**, *6*, 1788–1793.

(15) Schettino, V.; Chelli, R.; Marsili, S.; Barducci, A.; Faralli, C.; Pagliai, M.; Procacci, P.; Cardini, G. *Theor. Chem. Acc.* **2007**, *117*, 1105–1120.

(16) Putrino, A.; Sebastiani, D.; Parrinello, M. *J. Chem. Phys.* **2000**, *113*, 7102–7109.

(17) Sebastiani, D.; Parrinello, M. *J. Phys. Chem. A* **2001**, *105*, 1951–1958.

(18) Filippone, F.; Parrinello, M. *Chem. Phys. Lett.* **2001**, *345*, 179–182.

(19) Tongraar, A.; Liedl, K. L.; Rode, B. M. *J. Phys. Chem. A* **1998**, *102*, 10340–10347.

(20) Eichinger, M.; Tavan, P.; *et al.*, J. H. *J. Chem. Phys.* **1999**, *110*, 10452–10467.

(21) Tongraar, A.; Rode, B. M. *Chem. Phys. Lett.* **2001**, *346*, 485–491.

(22) Laio, A.; VandeVondele, J.; Rothlisberger, U. *J. Chem. Phys.* **2002**, *116*, 6941–6948.

(23) Morrone, J. A.; Tuckerman, M. E. *Chem. Phys. Lett.* **2003**, *370*, 406–411.

(24) Kritayakornupong, C.; Plankensteiner, K.; Rode, B. *J. Phys. Chem. A* **2003**, *107*, 10330–10334.

(25) Tongraar, A.; Rode, B. M. *Phys. Chem. Chem. Phys.* **2004**, *6*, 411–416.

(26) Biswas, P. K.; Gogonea, V. *J. Chem. Phys.* **2005**, *123*, 164114.

(27) Tongraar, A.; Rode, B. M. *Chem. Phys. Lett.* **2005**, *403*, 314–319.

(28) Laio, A.; Parrinello, M. *P NATL ACAD SCI USA* **2002**, *99*, 12562–12566.

(29) Iannuzzi, M.; Laio, A.; Parrinello, M. *Phys. Rev. Lett.* **2003**, *90*, 238302.

(30) Di Pietro, E.; Pagliai, M.; Cardini, G.; Schettino, V. *J. Phys. Chem. B* **2006**, *110*, 13539–13546.

(31) Bernasconi, M.; Chiarotti, G. L.; P, P. F.; *et al.*, M. P. *Phys. Rev. Lett.* **1997**, *78*, 2008–2011.

(32) Parrinello, M. *Comput. Sci. Eng.* **2000**, *2*, 22–27.

(33) Parrinello, M. *Solid State Comm.* **1997**, *102*, 107–120.

(34) Pagliai, M.; Cardini, G.; Righini, R.; Schettino, V. *J. Chem. Phys.* **2003**, *119*, 6655–6662.

(35) Narayanan, S.; Gottesfelf, S.; Zawodzinski, T. *Direct Methanol Fuel Cells*; Electrochemical Society, Novenber 2001.

(36) Whitacre, J.; Valdez, T.; Narayanan, S. *J. Electrochem. Soc.* **2005**, *152*, A1780–A1789.

(37) Seo, M.; Yun, Y.; Lee, J.; Tak, Y. *J. Power Sources* **2006**, *159*, 59–62.

(38) Yang, Y.; Liang, Y. C. *J. Power Sources* **2007**, *165*, 185–195.

(39) Wang, Z.; Yin, G.; Shao, Y.; Yang, B.; Shi, P.; Feng, P. *J. Power Sources* **2007**, *165*, 9–15.

(40) Morrone, J. A.; Tuckerman, M. E. *J. Chem. Phys.* **2002**, *117*, 4403–4413.

(41) Handgraaf, J.; van Erp, T.; Meijer, E. *Chem. Phys. Lett.* **2003**, *367*, 617–624.

(42) Handgraaf, J.-W.; Meijer, E. J. *J. Chem. Phys.* **2004**, *121*, 10111–10119.

(43) Tsuchida, E.; Kanada, Y.; Tsukada, M. *Chem. Phys. Lett.* **1999**, *311*, 236–240.

(44) Haughney, M.; Ferrario, M.; McDonald, I. R. *Mol. Phys.* **1986**, *88*, 849–853.

(45) Haughney, M.; Ferrario, M.; McDonald, I. R. *J. Phys. Chem.* **1987**, *91*, 4934–4940.

(46) Ladanyi, B. M.; Skaf, M. S. *Ann. Rev. Phys. Chem.* **1993**, *44*, 335–368.

(47) Jorgensen, W. L. *J. Am. Chem. Soc.* **1980**, *102*, 543–549.

(48) Pagliai, M.; Cardini, G.; Schettino, V. *J. Phys. Chem. B* **2005**, *109*, 7475–7481.

(49) Faralli, C.; Pagliai, M.; Cardini, G.; Schettino, V. *J. Phys. Chem. B* **2006**, *110*, 14923–14928.

(50) Faralli, C.; Pagliai, M.; Cardini, G.; Schettino, V. *Theor. Chem. Acc.* **2007**, *118*, 417–423.

(51) Faralli, C.; Pagliai, M.; Cardini, G.; Schettino, V. *J. Chem. Theory Comput.* **2008**, *4*, 156–163.

(52) Yamagami, M.; Wakita, H.; Yamaguchi, T. *J. Phys. Chem.* **1995**, *103*, 8174–8178.

(53) Watanabe, I. *J. Mol. Liq.* **1995**, *65/66*, 245–252.

(54) D'Angelo, P.; Di Nola, A.; Mangoni, M.; Pavel, N. *J. Chem. Phys.* **1996**, *104*, 1779–1790.

(55) Megyes, T.; Radnai, T.; Grósz, T.; Pálinkàs, G. *J. Mol. Liq.* **2002**, *101*, 3–18.

(56) Megyes, T.; Radnai, T.; Wakisaka, A. *J. Phys. Chem. A* **2002**, *106*, 8059–8065.

(57) Adya, A. K.; Kalugin, O. N. *J. Chem. Phys.* **2000**, *113*, 4740–4750.

(58) Ohtaki, H.; Radnai, T. *Chem. Rev.* **1993**, *93*, 1157–1204.

(59) Guillot, B.; Marteau, P.; Obriot, J. *J. Chem. Phys.* **1990**, *93*, 6148–6164.

(60) Kropman, M. F.; Bakker, H. J. *Science* **2001**, *291*, 2118–212.

(61) Kropman, M. F.; Bakker, H. J. *Chem. Phys. Lett.* **2002**, *362*, 349–352.

(62) Kropman, M. F.; Bakker, H. J. *Chem. Phys. Lett.* **2003**, *370*, 741–746.

(63) Kropman, M. F.; Bakker, H. J. *J. Am. Cem. Soc.* **2004**, *126*, 9135–9141.

(64) Omta, A. W.; Kropman, M. F.; Bakker, S. W. H. J. *Science* **2003**, *301*, 347–349.

(65) Hamm, P.; Lim, M.; Hochstrasser, R. M. *Phys. Rev. Lett.* **1998**, *81*, 5326–5329.

(66) Sprik, M.; Impey, R. W.; Klein, M. L. *Phys. Rev. Lett.* **1986**, *56*, 2326–2329.

(67) Martyna, G. J.; Klein, M. L. *J. Chem. Phys.* **1992**, *96*, 7662–7671.

(68) Merrill, G. N.; Webb, S.; Bivin, D. *J. Phys. Chem. A* **2003**, *107*, 386–396.

(69) Mundy, C. J.; Kuo, I.-F. W. *Chem. Rev.* **2006**, *106*, 1282–1304.

(70) García-Muruais, A.; Cabaleiro-Lago, E.; Hermida-Ramón, J.; Ríos, M. A. *Chem. Phys.* **2000**, *254*, 109–123.

(71) Cabarcos, O. M.; Weinheimer, C. J.; Martínez, T. J.; Lisy, J. M. *J. Chem. Phys.* **1999**, *110*, 9516–9526.

(72) Islam, M. S.; Pethrick, R. A.; Pugh, D. *J. Phys. Chem. A* **1998**, *102*, 2201–2208.

(73) Ayala, R.; Martínez, J. M.; Pappalardo, R. R.; Marcos, E. S. *J. Phys. Chem. A* **2000**, *104*, 2799–2807.

(74) Merkling, P. J.; Ayala, R.; Martínez, J. M.; Pappalardo, R. R. *J. Chem. Phys.* **2003**, *119*, 6647–6654.

(75) A. Öhrn and G. Karlström, *J. Phys. Chem. B* **2004**, *108*, 8452–8459.

(76) Wu, C.-C.; Wang, Y.-S.; Chandhuri, C.; Jiang, J. C.; Chang, H.-C. *Chem. Phys. Lett.* **2004**, *388*, 457–462.

(77) Tobias, D. J.; Jungwirth, P.; Parrinello, M. *J. Chem. Phys.* **2001**, *114*, 7036–7044.

(78) Lee, H. M.; Kim, D.; Kim, K. *J. Chem. Phys.* **2002**, *116*, 5509–5520.

(79) Lee, H. M.; Kim, K. *J. Chem. Phys.* **2001**, *114*, 4461–4471.

(80) Hall, R. J.; Hillier, I. H.; Vincent, M. A. *Chem. Phys. Lett.* **2000**, *320*, 139–143.

(81) Chandrasekhar, J.; Jorgensen, W. L. *J. Chem. Phys.* **1982**, *77*, 5080–5089.

(82) Chandrasekhar, J.; Spellmeyer, D. C.; Jorgensen, W. L. *J. Am. Chem. Soc.* **1984**, *106*, 903–910.

(83) Jardón-Valadez, E.; Costas, M. *J. Mol. Struct. (THEOCHEM)* **2004**, *677*, 227–236.

(84) Ayala, R.; Martínez, J. M.; Pappalardo, R. R.; Saint-Martín, H.; Ortega-Blake, I.; Marcos, E. S. *J. Chem. Phys.* **2002**, *117*, 10512–10524.

(85) Ayala, R.; Martínez, J. M.; Pappalardo, R. R.; Marcos, E. S. *J. Chem. Phys.* **2003**, *119*, 9538–9548.

(86) Ayala, R.; Martínez, J. M.; Pappalardo, R. R.; Marcos, E. S. *J. Chem. Phys.* **2004**, *121*, 7269–7275.

(87) Impey, R. W.; Madden, P. A.; McDonald, I. R. *J. Phys. Chem.* **1983**, *87*, 5071–5083.

(88) Impey, R. W.; Sprik, M.; Klein, M. L. *J. Am. Chem. Soc.* **1987**, *109*, 5900–5904.

(89) Sesé, G.; Guàurdia, E.; Padró, J. A. *J. Chem. Phys.* **1996**, *105*, 8826–8834.

(90) Sesé, G.; Padró, J. A. *J. Chem. Phys.* **1998**, *108*, 6347–6352.

(91) Åqvist, J. *J. Phys. Chem.* **1990**, *94*, 8021–8024.

(92) Guàrdia, E.; Martí, J.; García-Terrés, L.; Laria, D. *J. Mol. Liq.* **2005**, *117*, 63–67.

(93) Straatsma T. P. and Berendsen H. J. C., *J. Chem. Phys.* **1988**, *89*, 5876–5886.

(94) Sprik, M.; Klein, M. L.; Watanabe, K. *J. Phys. Chem.* **1990**, *94*, 6483–6488.

(95) Egorov, A. V.; Komolkin, A. V.; Chizhik, V. I.; Yushmanov, P. V.; Lyubartsev, A. P.; Laaksonen, A. *J. Phys. Chem. B* **2003**, *107*, 3234–3242.

(96) Lee, S. H.; Rasaiah, J. C. *J. Phys. Chem.* **1996**, *100*, 1420–1425.

(97) Spångberg, D.; Hermansson, K. *Chem. Phys.* **2004**, *300*, 165–176.

(98) Spångberg, D.; Hermansson, K. *J. Chem. Phys.* **119**, *14*, 7263–7281.

(99) Spångberg, D.; Rey, R.; Hynes, J. T.; Hermansson, K. *J. Phys. Chem. B* **2003**, *107*, 4470–4477.

(100) Carignano, M. A.; Karlström, G.; Linse, P. *J. Phys. Chem. B* **1997**, *101*, 1142–1147.

(101) Obst, S.; Bradaczek, H. *J. Phys. Chem.* **1996**, *100*, 15677–15687.

(102) Perera, L.; Berkowitz, M. *J. Chem. Phys.* **1991**, *95*, 1954–1963.

(103) Dang L. X., *J. Phys. Chem. A* **2004**, *108*, 9014–9017.

(104) Chang T-M. and Dang L. X., *Chem. Rev.* **2006**, *106*, 1305–1322.

(105) Chowdhuri, S.; Chandra, A. *J. Chem. Phys.* **2006**, *124*, 084507.

(106) Jancsò, G.; Bopp, P.; Heinzinger, K. *Z. Naturforsch* **1985**, *40a*, 1235.

(107) Jorgensen, W. L.; Chandrasekhar, J.; Madura, J. D.; Impey, R. W.; Klein, M. L. *J. Chem. Phys.* **1983**, *79*, 926–935.

(108) Jorgensen, W.; Severance, D. L. *J. Chem. Phys.* **1993**, *99*, 4233.

(109) Perera, L.; Berkowitz, M. L. *Z. Phys. D* **1993**, *26*, 166.

(110) Smith, D. E.; Dang, L. X. *J. Chem. Phys.* **1994**, *101*, 7873.

(111) Luzar, A.; Chandler, D. *Phys. Rev. Lett.* **1996**, *76*, 928–931.

(112) Lavanya M. and Bernasconi M. and Parrinello M., *J. Chem. Phys.* **1999**, *111*, 1588–1591.

(113) Silvestrelli, P. L.; Parrinello, M. *Phys. Rev. Lett.* **1999**, *82*, 3308–3311.

(114) Silvestrelli, P. L.; Parrinello, M. *J. Chem. Phys.* **1999**, *111*, 3572–3580.

(115) Peslherbe, G.; Ladanyi, B.; Hynes, J. *J. Phys. Chem. A* **2000**, *104*, 4533.

(116) Liu, Y.; Tuckerman, M. E. *J. Phys. Chem. B* **2001**, *105*, 6598–6610.

(117) Vuilleumier, R.; Sprik, M. *J. Chem. Phys.* **115**, *8*, 3454–3468.

(118) Brodskaya, E.; Lyubartsev, A. P.; Laaksonen, A. *J. Chem. Phys.* **2006**, *116*, 7879–7892.

(119) Gubskaya, A. V.; Kusalik, P. *J. Chem. Phys.* **2002**, *117*, 5290–5302.

(120) Guillot, B. *J. Mol. Liq.* **2002**, *101*, 219–260.

(121) Spångberg, D. Ph.D. thesis, Uppsala, 2003.

(122) Kuo, I.-F. W.; Mundy, C. J.; McGrath, M. J.; Siepmann, J. I.; VandeVondele, J.; Sprik, M.; Hutter, J.; Chen, B.; Klein, M. L.; Mohamed, F.; Krack, M.; Parrinello, M. *J. Chem. Phys. B* **2004**, *108*, 12990–12998.

(123) González, B. S.; Hernández-Rojas, J.; Wales, D. J. *Chemical Physics Letters* **2005**, *412*, 23–28.

(124) Todorova, T.; Seitsonen, A. P.; Hutter, J.; Kuo, I.-F. W.; Mundy, C. J. *J. Phys. Chem. B* **2006**, *110*, 3685–3691.

(125) Lee, H.-S.; Tuckerman, M. E. *J. Chem. Phys.* **2007**, *126*, 164501.

(126) Jorgensen, W. L.; Bigot, B.; Chandrasekhar, J. *J. Am. Chem. Soc.* **1982**, *104*, 4584–4591.

(127) Mark, D.; Heinzinger, K.; Palinkas, G.; Bako, I. *Z. Naturforsch* **1991**, *46a*, 887–897.

(128) Selegue, T.; Moe, N.; Draves, J. A.; Lisy, J. M. *J. Chem. Phys.* **1992**, *96*, 7268–7278.

(129) Masella, M.; Cuniasse, P. *J. Chem. Phys.* **2003**, *113*, 1866–1873.

(130) Guàrdia, E.; Pinzòn, R. *J. Mol. Liq.* **2000**, *85*, 33–44.

(131) Kim, H. *J. Mol. Struct. (THEOCHEM)* **2001**, *540*, 79–89.

(132) Krienke, H.; Fischer, R.; Barthel, J. *J. Mol. Liq.* **2002**, *98-99*, 329–354.

(133) Boese, A. D.; Chandra, A.; Martin, J. M. L.; Marx, D. *J. Chem. Phys.* **2003**, *119*, 5965–5980.

(134) Diraison, M.; Martyna, G. J.; Tuckerman, M. E. *J. Chem. Phys.* **1999**, *111*, 1096–1103.

(135) Carrillo-Tripp, M.; Saint-Martin, H.; Ortega-Blake, I. *J. Chem. Phys.* **2003**, *118*, 7062–7073.

(136) Robertson W. H. and Johnson M. A., *Annu. Rev. Phys. Chem.* **2003**, *54*, 173–213.

(137) Marzari, N.; Vanderbilt, D. *Phys. Rev. B* **1997**, *56*, 12847–12862.

(138) Silvestrelli, P. L.; Marzari, N.; Vanderbilt, D.; Parrinello, M. *Solid State Comm.* **1998**, *107*, 7–11.

(139) Silvestrelli, P. L. *Phys. Rev. B* **1999**, *59*, 9703 – 9706.

(140) Berghold, G.; Mundy, C. J.; Romero, A. H.; Hutter, J.; Parrinello, M. *Phys. Rev. B* **2000**, *61*, 10040–10048.

(141) Szefczyk, B.; Sokalski, W. A.; Leszczynski, J. *J. Chem. Phys.* **2002**, *117*, 6952–6958.

(142) Henkelman, G.; Arnaldsson, A.; Jónsson, H. *Comput. Mater. Sci.* **2006**, *36*, 354–360.

(143) Grabowski, S. J.; Sokalski, W. A.; Leszczynski, J. *Chem. Phys.* **2007**, *337*, 68–76.

(144) Parthasarathi, R.; Raman, S. S.; Subramanian, V.; Ramasami, T. *J. Phys. Chem. A* **2007**, *111*, 7141–7148.

(145) Sanville, E.; Kenny, S. D.; Smith, R.; Henkelman, G. *J. Comp. Chem.* **2007**, *28*, 899–908.

(146) Vener, M. V.; Egorova, A. N.; Fomin, D. P.; Tsirelson, V. G. *Chem. Phys. Lett.* **2007**, *440*, 279–285.

(147) Rodrìguez, J. I.; Bader, R. F.; Ayers, P. W.; Michel, C.; Götz, A. W.; Bo, C. *Chem. Phys. Lett.* **2009**, *472*, 149–152.

(148) Tang, W.; Sanville, E.; Henkelman, G. *J. Phys.: Condens. Matter* **2009**, *21*, 084204.

(149) Bader Charge Analysis, http://theory.cm.utexas.edu/bader/.

(150) Bader, R. F. W. *Atoms in Molecules - A Quantum Theory*; Oxford University Press: Oxford, 1990.

(151) Bader, R. F. W. *Chem. Rev.* **1991**, *91*, 893–928.

(152) Raugei, S.; Klein, M. L. *J. Am. Chem. Soc.* **2001**, *123*, 9484–9485.

(153) Raugei, S.; Klein, M. L. *J. Chem. Phys.* **2002**, *116*, 196–202.

(154) Tanida, H.; Sakane, H.; Watanabe, I. *J. Chem. Soc., Dalton Trans.* **1994**, 2321–2326.

(155) Laasonen, K.; Klein, M. L. *J. Am. Chem. Soc.* **1994**, *116*, 11620–11621.

(156) Laasonen, K. E.; Klein, M. L. *J. Phys. Chem. A* **1997**, *101*, 98–102.

(157) Heuft, J. M.; Meijer, E. J. *J. Chem. Phys.* **2003**, *119*, 11788–11791.

(158) Pagliai, M.; Raugei, S.; Cardini, G.; Schettino, V. *J. Mol. Struct. (THEOCHEM)* **2003**, *630*, 141–149.

(159) Marrone T. J.; Merz K. M. Jr., *J. Phys. Chem.* **1993**, *97*, 6524–6529.

(160) White, J.; Schwegler, E.; Galli, G.; Gygi, F. *J. Chem. Phys.* **2000**, *113*, 4668–4673.

(161) Ramaniah, L. M.; Bernasconi, M.; Parrinello, M. *J. Chem. Phys.* **1999**, *111*, 1587–1591.

(162) Shannon, R. D. *Acta Cryst.* **1976**, *A32*, 751–767.

(163) Chandler, D. *Introduction to modern statistical mechanics*; Oxford University Press: New York Oxford, 1987.

(164) Lee, S. H.; Cummings, P. T. *J. Chem. Phys.* **2000**, *112*, 864–869.

(165) Hawlicka, E.; Swiatla-Wojcik, D. *J. Chem. Phys. A* **2002**, *106*, 1336–1345.

(166) Svishchev, I. M.; Kusalik, P. G. *J. Chem. Phys.* **1993**, *99*, 3049–3058.

(167) Svishchev, I. M.; Kusalik, P. G. *J. Chem. Phys.* **1994**, *100*, 5165–5171.

(168) Khalack, J. M.; Lyubartsev, A. P. *J. Chem. Phys.* **2005**, *109*, 378–386.

(169) De la Peña, L. H.; Kusalik, P. G. *J. Am. Chem. Soc.* **2005**, *127*, 5246–5251.

(170) Dal Peraro, M.; Raugei, S.; Carloni, P.; Klein, M. L. *J. Am. Chem. Soc.* **2004**, Submitted.

(171) Bakó, I.; Hutter, J.; Pálinkás, G. *J. Chem. Phys.* **2002**, *117*, 9838–9843.

(172) Ikeda, T.; Hirata, M.; Kimura, T. *J. Chem. Phys.* **2003**, *119*, 12386–12392.

(173) Lightstone, F. C.; Schwegler, E.; Hood, R. Q.; Gygi, F.; Galli, G. *Chem. Phys. Lett.* **2001**, *343*, 549–555.

(174) Marx, D.; Sprik, M.; Parrinello, M. *Chem. Phys. Lett.* **1997**, *273*, 360–366.

(175) Naor, M. M.; Nostrand, K. V.; Dellago, C. *Chem. Phys. Lett.* **2003**, *369*, 159–164.

(176) Blumberger, J.; Sprik, M. *J. Phys. Chem. B* **2004**, *108*, 6529–6535.

(177) Blumberger, J.; Bernasconi, L.; Tavernelli, I.; Vuilleumier, R.; Sprik, M. *J. Am. Chem. Soc.* **2004**, *126*, 3928–3938.

(178) Lyubartsev, A. P.; Laasonen, K.; Laaksonen, A. *J. Chem. Phys.* **2001**, *114*, 3120–3126.

(179) Tuckerman, M.; Laasonen, K.; Sprik, M.; Parrinello, M. *J. Chem. Phys.* **1995**, *103*, 150–161.

(180) Krekeler, C.; Delle Site, L. *J. Phys.: Condens. Matter* **2007**, *19*, 192101.

(181) Radnai, T.; Kálmán, E.; Pollmer, K. *Z. Naturforsch* **1984**, *39a*, 464–470.

(182) Tamura, Y.; Spohr, E.; Heinzinger, K.; Pálinkás, G.; Bakó, I. *Ber. Bunsenges Phys. Chem.* **1992**, *96*, 147–158.

(183) Megyes, T.; Grósz, T.; Radnai, T.; Bakó, I.; Pálinkás, G. *J. Phys. Chem. A* **2004**, *108*, 7261–7271.

(184) Megyes, T.; Bálint, S.; I. Bakó, T. G.; Radnai, T.; Pálinkás, G. *Chem. Phys.* **2006**, *327*, 415–426.

(185) Richens, D. T. *The Chemistry of Aqua Ions*; Wiley, 1997.

(186) Schwenk, C. F.; Loeffler, H.; Rode, B. *Chem. Phys. Lett.* **2001**, *349*, 99–103.

(187) Masia, M.; Rey, R. *J. Chem. Phys.* **2005**, *122*, 094502.

(188) Jiao, D.; King, C.; Grossfield, A.; Darden, T.; Ren, P. *J. Phys. Chem. B* **2006**, *110*, 18553–18559.

(189) Ikeda, T.; Boero, M.; Terakura, K. *J. Chem. Phys.* **2007**, *126*, 034501.

(190) Lightstone, F. C.; Schwegler, E.; Allesch, M.; Gygi, F.; Galli, G. *Chem. Phys. Chem.* **2005**, *6*, 1745–1749.

(191) Marx, D.; Heinzinger, K.; Pálinkás, G.; Bakó, I. *Z. Naturforsch* **1991**, *46A*, 887–897.

(192) Palinkas, G.; Heinzinger, K. *Models in Chemistry* **1995**, *132*, 5–29.

(193) Parr, R. G.; Pearson, R. G. *J. Am. Chem. Soc.* **1983**, *105*, 7512–7516.

(194) Shannon, R. D.; Prewitt, C. *Acta Cryst.* **1969**, *B25*, 925–946.

(195) Fuentealba, P.; Parr, R. G. *J. Chem. Phys.* **1991**, *94*, 5559–5564.

(196) Ghanty, T.; Ghosh, S. *J. Phys. Chem.* **1994**, *98*, 9197–9201.

(197) CINECA - Consorzio Interuniversitario, http://www.cineca.it/.

(198) Goodman, M.; Listowsky, I. *J. Am. Chem. Soc.* **1962**, *84*, 3770–3771.

(199) Goodman, M.; Listowsky, I.; Masuda, Y.; Boardman, F. *Biopolymers* **1963**, *1*, 33–42.

(200) Nelson, J. W.; Kallenbach, N. R. *Proteins* **1986**, *1*, 211–217.

(201) Nelson, J. W.; Kallenbach, N. R. *Biochemistry* **1989**, *28*, 5256–5261.

(202) Buck, M.; Radford, S. E.; Dobson, C. M. *Biochemistry* **1993**, *32*, 669–678.

(203) Cammers-Goodwin, A.; Allen, T. J.; Oslick, S. L.; McClure, K. F.; Lee, J. H.; Kemp, D. S. *J. Am. Chem. Soc.* **1996**, *118*, 3082–3090.

(204) Bhattacharjya, S.; Balaram, P. *Protein Sci.* **1997**, *6*, 1065–1073.

(205) Buck, M. *Q. Rev. Biophys.* **1998**, *31*, 297–355.

(206) Bhattacharjya, S.; Venkatraman, J.; Kumar, A.; Balaram, P. *J. Peptide Res.* **1999**, *54*, 100–111.

(207) Khandelwal, P.; Seth, S.; Hosur, R. V. *Biophys. Chem.* **2000**, *87*, 139–148.

(208) Gerig, J. T. *Biopolymers* **2004**, *74*, 240–247.

(209) Gerig, J. T. *Biophys. J.* **2004**, *86*, 3166–3175.

(210) Lee, S.; Kim, Y. *Bull. Korean Chem. Soc.* **2004**, *25*, 838–842.

(211) Kemmink, J.; Creighton, T. E. *Biochemistry* **1995**, *34*, 12630–12635.

(212) Fioroni, M.; Burger, K.; Mark, A. E.; Roccatano, D. *J. Phys. Chem. B* **2000**, *104*, 12347–12354.

(213) Senent, M. L.; Perez-Ortega, A.; Arroyo, A.; Domínguez-Gómez, R. *Chem. Phys.* **2001**, *266*, 19–32.

(214) Takamuku, T.; Kumai, T.; Yoshida, K.; Otomo, T.; Yamaguchi, T. *J. Phys. Chem. A* **2005**, *109*, 7667–7676.

(215) Kuprin, S.; Gräslund, A.; Ehrenberg, A.; Koch, M. H. J. *Biochem. Biophys. Res. Commun.* **1995**, *217*, 1151–1156.

(216) Fioroni, M.; Burger, K.; Mark, A. E.; Roccatano, D. *J. Phys. Chem. B* **2001**, *105*, 10967–10975.

(217) Roccatano, D.; Fioroni, M.; Zacharias, M.; Colombo, G. *Protein Sci.* **2005**, *14*, 2582–2589.

(218) Wei, G.; Shea, J.-E. *Biophys. J.* **2006**, *91*, 1638–1647.

(219) Hilderbrandt, R. L.; Andreassen, A. L.; Bauer, S. H. *J. Phys. Chem.* **1970**, *74*, 1586–1592.

(220) Compton, D. A. C.; Goddard, J. D.; Hsi, S. C.; Murphy, W. F.; Rayner, D. M. *J. Phys. Chem.* **1984**, *88*, 356–363.

(221) Bhattacharjya, S.; Adiga, S. K. A. P. R.; Balaram, P. *Protein Sci.* **1998**, *7*, 123–131.

(222) Hong, D.-P.; Hoshino, M.; Kuboi, R.; Goto, Y. *J. Am. Chem. Soc.* **1999**, *121*, 8427–8433.

(223) Berkessel, A.; Adrio, J. A.; Hüttenhain, D.; Neudörfl, J. M. *J. Am. Chem. Soc.* **2006**, *128*, 8421–8426.

(224) Becke, A. D. *Phys. Rev. A* **1988**, *38*, 3098–3100.

(225) Lee, C.; Yang, W.; Parr, R. G. *Phys. Rev. B* **1988**, *37*, 785–789.

(226) Goedecker, S.; Teter, M.; Hutter, J. *Phys. Rev. B* **1996**, *54*, 1703–1710.

(227) Hartwigsen, C.; Goedecker, S.; Hutter, J. *Phys. Rev. B* **1998**, *58*, 3641–3662.

(228) Procacci, P.; Darden, T. A.; Paci, E.; Marchi, M. *J. Comput. Chem.* **1997**, *18*, 1848–1862.

(229) Hornak, V.; Abel, R.; Okur, A.; Strockbine, B.; Roitberg, A.; Simmerling, C. *Proteins* **2006**, *65*, 712–725.

(230) Anderson, D.; Terwilliger, T. C.; Wickner, W.; Eisenberg, D. *J.Biol.Chem.* **1980**, *255*, 2758–2582.

(231) Terwilliger, T. C.; Eisenberg, D. *J.Biol.Chem.* **1982**, *257*, 6010–6015.

(232) Terwilliger, T. C.; Eisenberg, D. *J.Biol.Chem.* **1982**, *257*, 6016–6022.

(233) Bernstein, F. C.; Koetzle, T. F.; Williams, G. J. B.; Meyer, E. F.; Brice, M. D.; Rogers, J. R.; Kennard, O.; Shimanouchi, T.; Tasumi, M. *J. Mol. Biol.* **1977**, *112*, 535–542.

(234) Marchi, M.; Procacci, P. *J. Chem. Phys.* **1998**, *109*, 5194–5202.

(235) Nosé, S. *Mol. Phys.* **1984**, *52*, 255–268.

(236) Nosé, S.; Klein, M. L. *Mol. Phys.* **1983**, *50*, 1055–1076.

(237) Czarnik-Matusewicz, B.; Pilorz, S.; Bieńko, D.; Michalska, D. *Vib. Spectrosc.* **2008**, *47*, 44–52.

(238) Schall, H.; t. Häber,; Suhm, M. S. *J. Phys. Chem. A* **2000**, *104*, 265–274.

(239) Czarnik-Matusewicz, B.; Pilorz, S.; Zhang, L.-P.; Wu, Y. *J. Mol. Struct.* **2008**, *883-884*, 195–202.

(240) Yoshida, K.; Yamaguchi, T.; Adachi, T.; Otomo, T.; Matsuo, D.; Takamuku, T.; Nishi, N. *J. Chem. Phys.* **2003**, *119*, 6132–6142.

(241) Gast, K.; Siemer, A.; Zirwer, D.; Damaschun, G. *Eur. Biophys. J.* **2001**, *30*, 273–283.

(242) Rajan, R.; Awasthi, S. K.; Bhattacharjya, S.; Balaram, P. *Biopolymers* **1997**, *42*, 125–128.

(243) Grossman, J. C.; Schwegler, E.; Draeger, E. W.; Gygi, F.; Galli, G. *J. Chem. Phys.* **2004**, *120*, 300–311.

(244) Schwegler, E.; Grossman, J. C.; Gygi, F.; Galli, G. *J. Chem. Phys.* **2004**, *121*, 5400–5409.

(245) Prendergast, D.; Grossman, J. C.; Galli, G. *J. Chem. Phys.* **2005**, *123*, 014501.

(246) Hajdu, F.; Lengyel, S.; Pálinkás, G. *J. Appl. Cryst.* **1976**, *9*, 134–138.

(247) Soper, A. K. *Chem. Phys.*. **2000**, *258*, 121–137.

(248) Duan, Y.; Wu, C.; Chowdhury, S.; Lee, M. C.; Xiong, G.; Zhang, W.; Yang, R.; Cieplak, P.; Luo, R.; Lee, T.; Caldwell, J.; Wang, J.; Kollman, P. *J. Comput. Chem.* **2003**, *24*, 1999–2012.

(249) Cancès, E.; Mennucci, B.; Tomasi, J. *J. Chem. Phys.* **1997**, *107*, 3032–3041.

(250) Mennucci, B.; Tomasi, J. *J. Chem. Phys.* **1997**, *106*, 5151–5158.

(251) Mennucci, B.; Cancès, E.; Tomasi, J. *J. Phys. Chem. B* **1997**, *101*, 10506–10517.

(252) Tomasi, J.; Mennucci, B.; Cancès, E. *J. Mol. Struct. (THEOCHEM)* **1999**, *464*, 211–226.

(253) Hirota-Nakaoka, N.; Goto, Y. *Bioorg. Med. Chem.* **1999**, *7*, 67–73.

(254) Habermann, E. *Science* **1972**, *117*, 314–322.

(255) Cecchi, L.; De Sarlo, F.; Machetti, F. *Eur. J. Org. Chem.* **2006**, 4852–4860.

(256) Machetti, F.; Cecchi, L.; Trogu, E.; De Sarlo, F. *Eur. J. Org. Chem.* **2007**, 4352–4359.

(257) Trugu, E.; De Sarlo, F.; Machetti, F. *Chem. Eur. J.* **2009**, *15*, 7940–7948.

(258) Glukhovtsev, M. N.; Bach, R. D.; Pross, A.; Radom, L. *Chem. Phys. Lett.* **1996**, *260*, 558–564.

(259) Frisch *et al.*, *Gaussian 98, Revision A.11*; Gaussian Inc.: Pittsburg, PA, 1998.

(260) Schmidt, M. W.; Baldridge, K. K.; Boatz, J. A.; Elbert, S. T.; Gordon, M. S.; Jensen, J. H.; S. Koseki and, N. M.; Nguyen, K. A.; Su, S.; Windus, T. L.; Dupuis, M.; Montgomery, J. A. *J. Comput. Chem.* **1993**, *14*, 1347–1363.

(261) Dykstra, C. E.; Frenking, G.; Kim, K. S.; Scuseria, G. E. *Theory and Applications of Computational Chemistry: the first forty years*; Elsevier: Amsterdam, 2005.

(262) Corsico Coda, A.; Desimoni, G.; Gamba, A.; Invernizzi, G.; Righetti, P. P.; Seneci, P. F.; Tacconi, G. *Gazz. Chim. Ital.* **1985**, *115*, 111–118.

(263) Von Deuten, K.; Hinrichs, W.; Klar, C. *Polyhedron* **1982**, *1*, 247–251.

(264) Smernik, J.; Oades, J. M. *J. Environ. Qual.* **2002**, *31*, 414–420.

(265) Møller, C.; Plesset, M. S. *Phys. Rev.* **1934**, *46*, 618–622.